Meissner Levitating Micro Particle as a gravitational force sensor

van Halteren, Noud

Citation

Van Halteren, N. (2022). *Meissner Levitating Micro Particle as a gravitational force sensor*.

Meissner Levitating Micro Particle as a gravitational force sensor

THESIS

submitted in partial fulfillment of the
requirements for the degree of

BACHELOR OF SCIENCE
in
PHYSICS

Author :	N.T.R. van Halteren
Student ID :	S2003627
Supervisor :	Prof.dr.ir. T.H. Oosterkamp
2^{nd} corrector :	Dr. W. Löffler

Leiden, The Netherlands, July 4, 2022

Meissner Levitating Micro Particle as a gravitational force sensor

N.T.R. van Halteren

Huygens-Kamerlingh Onnes Laboratory, Leiden University
P.O. Box 9500, 2300 RA Leiden, The Netherlands

July 4, 2022

Abstract

In an effort to bring quantum mechanics and general relativity closer to each other the Oosterkamp group is developing a gravitational force sensor. This gravitational force sensor is a micromechanical resonator. This resonator consist of a superconducting confinement and a micro particle, the zeppelin. This zeppelin weighs a mere 0.433mg and consists mainly of neodymium magnets, which due to the Meissner effect will levitate. This brings gravity into the equation, and allows for gravitational manipulation of the zeppelin. This manipulation is achieved using a mass wheel with three blocks of approximately 2.4 kg attached to it. The interactions of these masses with the zeppelin can be measured using a SQUID. The zeppelin is free to move in all six degrees of freedom and also vibrates in all six. The theoretical dependencies of these motions are used to construct a zeppelin, such that the vibrations produced are in a preferred range. After several runs in which the vibration isolation was improved and several different zeppelins were used, run28 was produced. Run28 produced a beautiful spectrum. This eventually led up to gravitational measurements on a mode with a frequency of 26.69 Hz. Of this mode the Q-factor and energy coupling are determined at $9.13 \cdot 10^6$ and $2.46 \cdot 10^{-6}$ respectively. These are both used in the calibration of the experiment, the sensitivity. This allows for the signal to be converted from voltage to newtons. This is the highest Q-factor yet measured by the Oosterkamp group on this experiment. The gravitational measurements are done with the mass wheel on several different position after what appeared as a first signal was measured. The measurements kept on producing signals. After which an extensive data analysis is performed on the data points generated by the measurements.

This data analysis compares simulations to the measured data points. It remains hard to conclude which mode of vibration is measured, due to several short comings in the current possible execution of the experiment. Several improvements on the execution of the experiment and the expectations are needed for this to be possible. Nevertheless with confidence it can be said that repeatedly gravitational signals are measured of the order of several tens of attonewtons of force.

Contents

Version of July 4, 2022– Created July 4, 2022 - 18:59

Chapter 1

Introduction

1.1 The gap

In physics unification of theories is of great importance, since this connects how we see and interpret the physical world. The grand goal therefore is complete unification of physics, an all encompassing ”Theory of everything”. There exist a gap which prevents the completion of this unification, this gap lies between general relativity and quantum mechanics. Two enormously successful theories which are widely used, validated and accepted.

These theories are however vastly different in their nature and description. While quantum mechanics describes everything about interactions and phenomena on the smallest of scales, general relativity on the contrary concerns gravitational interactions on vast scales. These theories therefore rarely are relevant simultaneously, since the context in which they are relevant vastly differ. There are however small niches, right at the limit of both theories, where both theories could be valid and this is where physicist search for quantum gravity.

When the limit of quantum mechanics is pushed to ever larger scales and that of general relativity to ever smaller scales, the two theories would have to meet at some point. Pushing these limits is effectively closing the gap, to the possibility of a bridge between these theories. Most research on this topic focuses on the idea of creating heavy superpositions, since superpositions fall under quantum mechanics and when things become heavy enough general relativity comes in to play. Lots of previous research focuses on the Planck scale, yet new upcoming research introduced a shift in this field and more research is now looking at a new potential bridge, the micromechanical resonator.

1.2 Levitating particle

One such a micromechanical resonator is a levitating particle, in these systems gravity is countered by a levitating force. This levitating force can be experimentally controlled, allowing a certain amount of control over the potential. Furthermore systems like this can be environmentally controlled to reduce noise and dissipation, which can be achieved by cooling down to cryogenic temperatures and the use of a vacuum. This greatly increases the quality (Q) factor of the system, through reduction of damping factors.

A super sensitive force sensor, using this levitating particle concept can be developed to start closing the gap with extremely sensitive gravity measurement on small scale. This means that the limit which is looked is the lower gravitational limit. The Oosterkamp research group at first developed the so called *"Lead Zeppelin"*, which was a lead particle that was kept afloat and confined using a magnetic field[1]. Vinante et al. had different, reversed, roles for the particle and the confinement. The particle is the source of the magnetic field, which is static in this case, and the confinement is a superconducting lead trap. For this experiment they achieved a promising Q-factor of the order of 10^7 at relative high temperature and pressure[2]. Following this development the Oosterkamp group adapted their experimental setup to one of similar kind, and that will be the subject of this thesis.

The eventual preliminary goal is to develop and study this system to such a degree that it is possible to look a the effects of gravity, or thermal motion, on a small scale. This is easiest when all six modes of vibration, including this vertical-mode, belonging to the six degree's of freedom are characterised. Then the vertical mode can be isolated for gravitational measurements on gravitational effects such as those of a gravitational wheel or from tidal forces of the moon and sun.

These effects and several others will be explained further in the theory section of this thesis, complementary to this will be the methods section which deals with the more practical side of the theory's application in this research. Such as the measurement device, SQUID, which is capable of measuring such small vibrations. Eventually leading up to the results and the interpretation of the results will be discussed. At last, a conclusion will be made with an outlook on what can be a suitable follow-up research concerning the eventual goal of trying to close the gap between quantum mechanics and gravity.

Chapter 2

Theory

This chapter will further elaborate upon all the relevant theories concerning this research, expanding on what was mentioned in the introduction. The aim is to provide a more in depth understanding of the underlying physics of the phenomena which are studied.

2.1 Gravity

Gravity is the weakest of the four fundamental forces of nature and was first described by Newton, which is now known as Newtonian gravity. Later Einstein described gravity in a revolutionary new way in his work on General relativity, which could be applied beyond the scope of Newtonian gravity. In this thesis gravity is seen as Newtonian gravity because at the small scale and in low gravity field the two theories are in agreement with each other, thus the simpler Newtonian gravity will be used.

2.1.1 Newtonian gravity

Newton introduced gravity as a force acting between two bodies with mass M and m, over a distance, r, which he formulated in his law of universal gravity:

$$F_G = G\frac{mM}{r^2} \tag{2.1}$$

Using Newton's second law of motion we can equate (2.1) and solve for an acceleration.

$$a_G = G\frac{M}{r^2} \tag{2.2}$$

When approximating earth as a perfect sphere with a uniform mass distribution this is a constant called the gravitational acceleration constant. With a standard definition of $g = 9.80665$, a note must be made that g actually isn't constant since gravity on earth does vary. Due to the sensitivity of this experiment this must be kept in mind. Using this equation (2.1) can be simplified to the following:

$$F_g = mg \tag{2.3}$$

Now making the step towards an energy description the gravity potential can be introduced. In general a conservative force, meaning path independent force, can be written as the gradient of a potential. In one-dimension this translate to a single derivative, which will be taken in the z-direction.

$$F_g = mg = \frac{dU_g}{dz} \tag{2.4}$$

Using simple rules of integration this leads us to the potential for gravity.

$$U_g = mgz \tag{2.5}$$

This potential will resurface when the complete potential will be assembled, which will describe the behaviour of our levitating particle.

2.2 Superconductors

This section will touch upon the physics happening in and around superconductors, to establish a understanding of how they work. This will be brought about by explaining the general concept of superconductors and differentiating between the two main types of superconductors. Furthermore the concepts of (super)diamagnetism and the Meissner effect will be set out in depth.

2.2.1 Types of superconductors

Superconductors in general

A superconductor is material that can exhibit superconductivity when certain critical conditions are met. Superconductivity is a material property where all electrical resistance disappears and magnetic fields are expelled from within the material, this last property is known as the superdiamagnetism. This phenomenon occurs spontaneously during the phase transition, this is known as the Meissner effect. This effect plays a critical role in this research.

Superconductivity occurs for certain materials when the correct conditions are met. When these conditions are met a transitions occurs, this happens typically for low temperature and low magnetic field. The transition temperature is known as the critical temperature (T_c) and the transition field is known as the critical field (B_c). It must be noted that for most (metallic) conductors in general the electrical resistance drops with temperature, however never fully reaches absolute zero.

There are two main types of superconductors, type-I and type-II. While they both follow the general concept of superconductivity, they differ in how they respond to a magnetic field. Further distinction between these types of superconductors is made below with reference to figure 2.1.

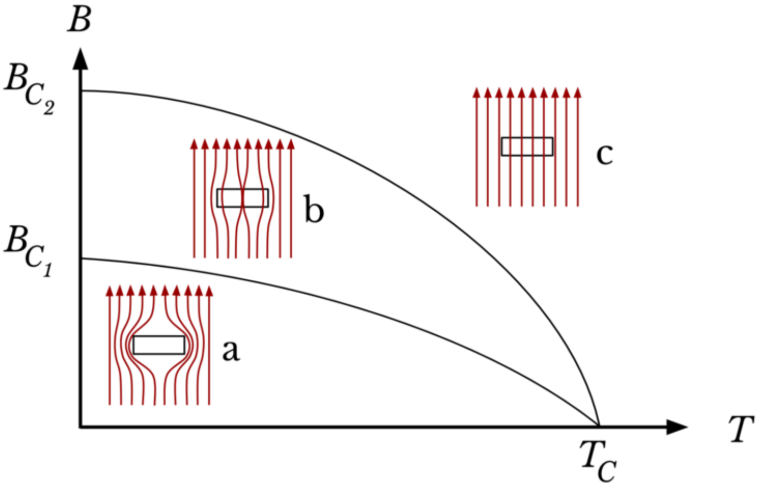

Figure 2.1: *Phase transition graph of a type-II superconductor. Showing the magnetic flux as a function of the temperature, making clear distinction between three area's (a, b and c). Where area "a" is the superconducting Meissner state, area "b" is a mixed state and area "c" is the normal state. Furthermore the critical temperature (T_c) and critical field values (B_{C_1}, B_{C_2}) are displayed.*[3]

Type-I superconductor

A type-I superconductor can be seen as the regular simple superconductor, it has one clear phase transition from a normal state to a superconducting Meissner state. This means a type-I only has one transition line between

B_C and T_C, since it has only one B_C. This means that a phase transition graph would look like figure 2.1, only without the existence of area ″b″, B_{C_2} and the upper transition line.

type-II superconductor

A type-II superconductor has a more complex form of diamagnetism. Its behaviour is split into three phases, as shown in figure 2.1, since a type-II contrary to a type-I has an intermediate phase preceding its regular superconductive phase. In this phase small magnetic vortices are present, where some of the field lines converge and penetrate through the material. This is shown in figure 2.1 as the behaviour present in area ″b″. Here intermediate behaviour depends on the values of the field and the temperature. Below this phase a type-II superconductor acts as a type-I superconductor and the Meissner effect always occurs.

2.2.2 Meissner effect and superdiamagnetism

The Meissner effect is the spontaneous expulsion of magnetic fields during the transition of materials to their superconducting state due to what is known as superdiamagnetism. This section will further explain how this effect occurs and section 2.4 will expand upon this on how these phenomena lead to levitation.

Superdiamagnetism

To understand superdiamagnetism normal diamagnetism must be understood. Diamagnetism is a type of magnetism where the dipole moments of the electrons align anti-parallel to an external magnetic field, inducing an opposing magnetic field. Diamagnetism is typically very weak and only dominant when the are no other contributions to the magnetism. Diamagnetism is present is all materials, however in many materials other forms of magnetism dominate. The diamagnetism in superconductor is called superdiamagnetism, since it is a strong form of diamagnetism which is nearly perfect. Therefore superconductors are sometimes called perfect diamagnets. The diamagnetism of a superconductor fully expels magnetic fields everywhere in the material apart from a thin layer. In this thin layer the field reduces from the external value to zero. How quickly this happens depends on the London penetration depth.

London penetration depth

As mentioned before the London penetration depth characterises how quickly an external magnetic field reduces when it enters a superconductor. The smaller the value the thinner the layer in which an external magnetic field penetrates a superconductor. This behaviour is captured in the following equation:

$$B(d) = B_0 \exp\left(\frac{-d}{\lambda_L}\right) \tag{2.6}$$

Where *B(d)* represents the magnitude of the internal magnetic field on depth d for $0 \leq d < \infty$, B_0 is the value of the field on entering the superconductor at d = 0 and λ_L is known as the London penetration depth. This depth is defined as the depth for which the field has reduced by a factor of $1/e$ and is given by the following equation:

$$\lambda_L = \sqrt{\frac{m}{\mu_0 n_e e^2}} \tag{2.7}$$

For the derivation of both these equations see appendix A.1.

Thus superconductors always have a thin layer on their surface in which they are ”normal”, normal meaning not superconducting. This layer is typically of the order of 10 or 10^2 nm, which compared to macro scale materials is extremely small. This layer is shown in figure 2.2 consistent with equation 2.6.

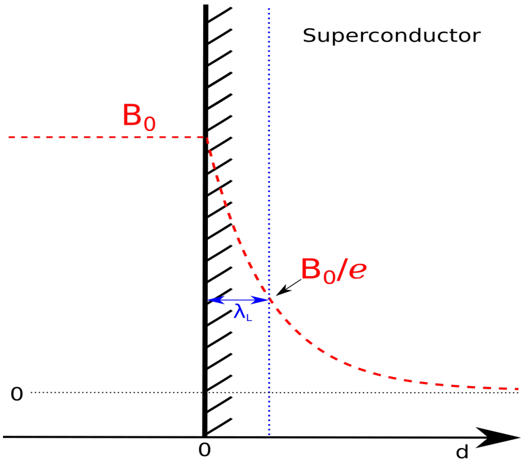

Figure 2.2: *Schematic showing how external fields decreases inside a superconductor and how the London penetration depth is defined.*

2.3 Eddy currents

When a conductor is present within a changing magnetic field so called Eddy currents are induced in the conductor. These Eddy currents are current loops induced according to one of the Maxwell equations, the law of induction. This law is also known as Faraday's law and can be seen below.

$$\nabla \times \mathbf{E} = -\frac{\partial \mathbf{B}}{\partial t} \tag{2.8}$$

This equation 2.8 shows that the currents flows perpendicular to the fields, since there is a cross product present. These currents induce their own magnetic field which opposes the changing magnetic field. In this manner a magnetic dipole is formed in the (super)conductor. This induced opposing field is similar to the opposing field seen with (super)diamagnetism, however this field is due to a changing field not a static field.

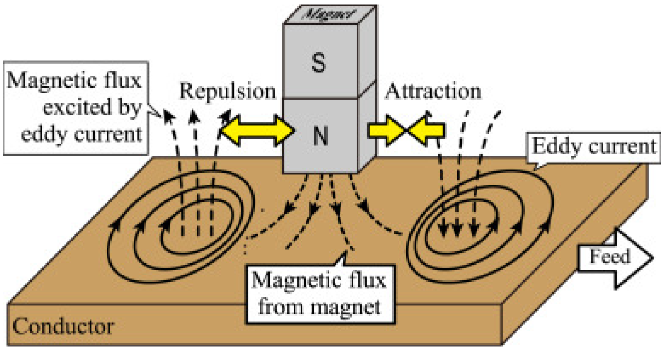

Figure 2.3: *Schematic showing how the magnetic flux from a magnet induces eddy currents in a moving conductor, which on their turn again excite a magnetic flux. Which can have repulsive and attractive effects on the magnet.*[4]

What differentiates Eddy current in a superconducting surface versus a normal surface is the following. In a superconducting layer these currents loops would encounter no resistance and persist without any energy loss, so once formed they are maintained and with them the magnetic dipole.

2.4 Dipole induced levitation

Now the question arises how the behaviour of a superconductor can lead to levitation. This section will use the introduced physics and derive the interaction which causes the levitation and confinement.

2.4.1 Mirror dipoles

The main source of levitation are the magnetic dipoles and their fields, these act out a repulsive force. A superconductor nearly perfectly opposes any external field and thus creates a strong repulsive force. A general method to approach and model this is known as the method of images. A magnet above a superconducting surface, as is the case in our experiment, can be modeled using this image method. The image method is a method where the magnetic dipole of the magnet is mirrored by the superconducting surface, leading to image dipoles. As a result, no field lines cross the surface of the supercodnuctor. Instead all field lines run parallel to the surface.

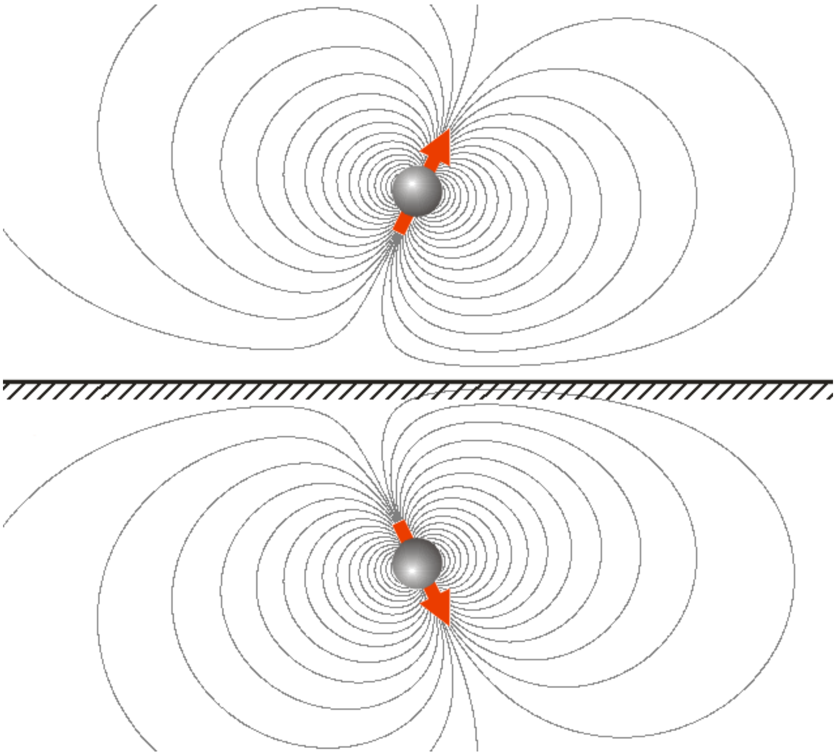

Figure 2.4: *Figure showing the mirror image method.*[5]

2.4.2 Dipole with mirror dipole interaction

Using the image method, the repulsion can be calculated as two interacting dipoles. The field for the magnetic dipole $(\mathbf{m_1})$ is given by Griffiths[6]:

$$\mathbf{B}_{dip}(\mathbf{r}) = \frac{\mu_0}{4\pi}\frac{1}{r^3}[3(\mathbf{m_1}\cdot\hat{\mathbf{r}})\hat{\mathbf{r}} - \mathbf{m_1}] + \frac{2\mu_0}{3}\mathbf{m_1}\delta^3(\mathbf{r}) \tag{2.9}$$

The $\frac{2\mu_0}{3}\mathbf{m_1}\delta^3(\mathbf{r})$ term makes sure that the fourth Maxwell equation, $\nabla \times \mathbf{B} = 0$, holds. Normally the energy of a dipole in a magnetic field is given by $U = -\mathbf{m}\cdot\mathbf{B}$. However one of the dipoles is an image and the field inside the superconductor is zero. This reduces the energy by a factor half, leading to:

$$U = -\frac{1}{2}\mathbf{m_2}\cdot\mathbf{B} \tag{2.10}$$

Therefore the interaction energy for a dipole interaction between a dipole $(\mathbf{m_1})$ with a mirror dipole $(\mathbf{m_2})$ is given by:

$$U(\mathbf{r}) = -\frac{\mu_0}{8\pi}\frac{1}{|\mathbf{r}|^3}[3(\mathbf{m_1}\cdot\hat{\mathbf{r}})(\mathbf{m_2}\cdot\hat{\mathbf{r}}) - \mathbf{m_1}\cdot\mathbf{m_2}] - \frac{\mu_0}{3}\mathbf{m_1}\cdot\mathbf{m_2}\delta^3(\mathbf{r}) \tag{2.11}$$

The last term will always vanish in this situation, since $(\mathbf{m_1})$ and $(\mathbf{m_2})$ cannot be exactly on top of each other, the equation will simplify to:

$$U(\mathbf{r}) = -\frac{\mu_0}{8\pi}\frac{1}{|\mathbf{r}|^3}[3(\mathbf{m_1}\cdot\hat{\mathbf{r}})(\mathbf{m_2}\cdot\hat{\mathbf{r}}) - \mathbf{m_1}\cdot\mathbf{m_2}] \tag{2.12}$$

2.5 Harmonic oscillators

The concept of the harmonic oscillator is both used classical and quantum mechanical, since any smooth potential can be approximated as an harmonic oscillator around a certain minimum. Such a minimum is generally a stable equilibrium point. In this thesis the classical harmonic oscillator will be discussed and is relevant for several parts of the experiment. The potential describing the behaviour of our levitating particle will be approximated as a harmonic oscillator. Furthermore, the vibration isolation used in this experiment consists of mass-spring systems. These are also well described by harmonic oscillators.

2.5.1 The classical harmonic oscillator

In classical mechanics there are three distinct harmonic oscillators, the simple harmonic oscillator, the damped harmonic oscillator and the driven harmonic oscillator. These essentially expand upon each other and will be discussed in this order, introducing important concepts along the way.

Simple harmonic oscillator

The simple harmonic oscillator finds it purpose in modeling any simple linear restoring force without any form of damping or driving force. Consequently this restoring force is simply equated with Newton's second law. This will be realized in one dimension for an arbitrary variable r, which can be any one of the six degree's of freedom.

$$F = m\ddot{r} = -k_r r \tag{2.13}$$

Where k_r is a constant connected to the restoring force in the direction of r. The potential energy belonging to this restoring force is:

$$U_r = \frac{1}{2} k_r r^2 \tag{2.14}$$

Equation 2.13 can be rewritten into an equation of motion.

$$m\ddot{r} + k_r r = 0 \tag{2.15}$$

$$\ddot{r} + \omega_0^2 r = 0 \tag{2.16}$$

where $\omega_0 = \sqrt{\frac{k_r}{m}}$ is known as the undamped angular frequency, also known as the natural frequency. This equation of motion has a simple general solution of the form:

$$r(t) = A \cdot \cos(\omega_0 t + \phi) \tag{2.17}$$

Damped harmonic oscillator

In any almost any system there is always some sort of friction or loss from an other form of dissipation. This can be modeled as damping, this will be modeled as a opposing force proportional to the velocity.

$$F_{friction} = -c\dot{r} \tag{2.18}$$

Here c is the proportional factor which is dependent on the object and the medium. The definition of the potential energy remains the same since friction is a non-conservative force. The potential does change due to the fact that the equation of motion will be different. Therefore the solution of the equation of motion (r(t)), which leads to a different potential (U_r, equation 2.14).

This new damping force now expands the simple harmonic oscillator to a damped oscillator with the next equation of motion:

$$m\ddot{r} + c\dot{r} + k_r r = 0 \tag{2.19}$$

Now introducing a new quantity $\gamma = \frac{c}{2mw_0}$, the damping factor, we arrive at the equation of motion:

$$\ddot{r} + 2\gamma\omega_0\dot{r} + \omega_0^2 r = 0 \tag{2.20}$$

There are three distinct scenario's depending on the value of γ, these are the following: Overdamped ($\gamma > 1$), critically damped (γ=1) and underdamped ($\gamma < 1$). For this thesis the underdamped scenario will be relevant. This is because of the controlled environment of the experiment where damping factors are extremely low. The underdamped harmonic oscillator has the following solution:

$$r(t) = A \cdot \sin\left(\sqrt{1-\gamma^2}\omega_0 t + \phi\right) \cdot e^{-\gamma\omega_0 t} \tag{2.21}$$

We again see a sinusiodal solution, whose angular frequency is now modulated by the damping. This is the damped angular frequency, $\omega_d = \sqrt{1-\gamma^2}\omega_0$. Two other quantaties can be introduced here, namely the Q-factor and the relaxation time tau, τ. The Q-factor is known as the quality factor and has two different definitions. The two types of definitions are both relevant in the case of a resonator, however depending on context one or the other is more relevant. The first definitions is more relevant when talking about peaks in a spectrum due to the resonances.

$$Q = \frac{f_{res}}{f_{FWHM}} = \frac{\omega_{res}}{\Delta\omega} \tag{2.22}$$

Where f_{res} is the resonance frequency and f_{FWHM} is the Full Width at Half Maximum, which is the peaks width at half the peak value.

The second definition is in the context of energy and how quick is dissipates. This is good definition when talking about the damping of a system. These two different definitions of Q become roughly the same when the Q-factor is high enough. For this experiment Q is considered high enough.

$$Q = 2\pi \cdot \frac{\text{Energy stored}}{\text{Energy lost per cycle}} = \frac{mw_{res}}{c} = \frac{1}{2\gamma} \tag{2.23}$$

Now it is necessary to introduce the concept of resonance. Any of the modes belonging to one of the degrees of freedom have a certain frequency for which it's amplitude response is the biggest. This frequency for which a system resonates at maximum amplitude, is known as the resonant frequency and it is defined as $\omega_{res} = \sqrt{1-2\gamma^2}\omega_0 = \sqrt{1-\frac{1}{2Q^2}}\omega_0$.

It must be noted that for an underdamped system with very low γ that ω_d and ω_{res} are both really close to ω_0, and ω_0 can be calculated. For low enough damping/high enough Q-factor then can be seen as equal. What is also important to realize is the fact that the frequencies of the modes can shift a little. This is due to the fact that γ is not constant enough on the scale of frequency resolution we are aiming for. Next to this also nonlinear behaviour can influence this, the frequencies can shift due to the amplitude.

Now a characteristic time is defined as tau (τ). Tau is defined, very similar to the London penetration depth, as the time needed for the amplitude to reduce with a factor e^{-1}. Looking at the exponential term in equation 2.21, this now leads to a simple equation for tau.

$$\tau = \frac{1}{\gamma\omega_0} \approx \frac{1}{\gamma\omega_{res}} \tag{2.24}$$

With this tau can be determined experimentally. Since it can be extracted from a ringdown measurement, which will later be introduced and of which a simple example is contained in the results chapter in section 4.2.1. From this also the Q-factor can be determined since equation 2.24 can be plugged into equation 2.23 leading to.

$$Q = \frac{1}{2}\omega_{res}\tau = \pi f_{res}\tau \tag{2.25}$$

Tau is thus a measure for the Q-factor.

Driven harmonic oscillator

For energy to be put into the system a driving force needs to be introduced, this is introduced as an external force. This contains all the external forces which work on the resonator. The equation of motion now becomes the following:

$$m\ddot{r} + c\dot{r} + k_r r = F_{ext}(t) \tag{2.26}$$

Now using the concept of Fourier transforms a transfer function can be calculated from this equation of motion, this will later be used to convert the units of the raw data. The transfer function is defined as:

$$H(\omega) = \frac{Output(\omega)}{Input(\omega)} = \frac{R(\omega)}{F(\omega)} \tag{2.27}$$

Where $R(\omega)$ and $F(\omega)$ are the Fourier transforms of $r(t)$ and $F(t)$ respectively. For a Fourier transformations the following holds: If $G(\omega)$ is the transform of g(t) then $i\omega G(\omega)$ is the transform of g′(t). Applying this to the equation of motion 2.26 results into.

$$-m\omega^2 R(\omega) + ic\omega R(\omega) + k_r R(\omega) = F_{ext}(\omega) \tag{2.28}$$

Which can be rewritten into the transfer function in the next steps:

$$(-m\omega^2 + ic\omega + k_r)R(\omega) = F_{ext}(\omega)$$

$$H(\omega) = \frac{R(\omega)}{F_{ext}(\omega)} = \frac{1}{-m\omega^2 + ic\omega + k_r}$$

Dividing by $1/k_r$ and using previous identities we arrive at the final form of our transfer function.

$$H(\omega) = \frac{1/k_r}{1 - (\frac{\omega}{\omega_0})^2 + i\frac{(\frac{\omega}{\omega_0})}{Q}} \tag{2.29}$$

This transfer function characterises how our system converts force into motion and can thus be used to convert the measured motion back in to force.

2.6 Calibration

An important part in the experiment is calibration. This simple means that measured signal can be converted to the correct amount of motion of the zeppelin. This is called the sensitivity [m/V], allowing to convert the measured voltage to a displacement. Which then on its turn can be converted to the corresponding amount of newtons. Calibration of a mode is done based on energy coupling between the zeppelin and the circuit. The energy coupling can be determined from a magnetic drive.

A magnetic drive is a drive due to the induced flux generated in the calibration coil. This acts out a electromotive force on the zeppelin. This happens 90 degrees out of phase due to the nature of such a force. Thus at resonance, the resultant motion is 90 degrees out of phase with the force, and hence 90 degrees out of phase with the current sent.

Such a drive allows to look at the response of the system with respect to how much is send in during the drive. From this the coupling can be determined. The coupling is defined as:

$$\beta^2 = \frac{\text{Electrical energy in the circuit}}{\text{Kinetic energy of the zeppelin}} = \frac{L_{tot} I^2}{k_r r^2} \tag{2.30}$$

Where L_{tot} is the total inductance of the circuit and I the current.
It turns out that $Q\beta^2$ is given by:

$$Q\beta^2 = \frac{\Delta\Phi_{zeppelin}}{\Phi_{drive}} \tag{2.31}$$

Since the coupling and the Q-factor directly relate the two systems response to each other. However for a measurement the time driven is a certain interval which isn't necessarily equal to τ. Therefore an effective Q-factor is defined for this time interval, t_{eff}. Q_{eff} is calculated in the same way as Q, which gives us several options to calculate Q_{eff}:

$$Q_{eff} = \frac{1}{2}\omega_{drive} t_{eff} = \pi f_{drive} t_{eff} = Q\frac{t_{eff}}{\tau} \tag{2.32}$$

Q_{eff} also holds for the equation 2.31, since a longer drive would increase the motion in the zeppelin as it would increase the Q. A longer drive doesn't mean more coupling, this remains constant. Now using Q_{eff} instead of Q, we arrive at:

$$Q_{eff}\beta^2 = \frac{\Delta\Phi_{zeppelin}}{\Phi_{drive}} \tag{2.33}$$

The flux response are directly related to the read out signal in volts, since the SQUID converts the flux proportionally with a conversion factor $\frac{V}{\Phi_0}$. This holds for both the fluxes equally and thus factors out, leading to:

$$Q_{eff}\beta^2 = \frac{\Delta V_{zeppelin}}{V_{drive}} \tag{2.34}$$

Where $\Delta V_{zeppelin}$ is the change in the voltage of the motion of the zeppelin, which is the difference between before and after the drive. V_{drive} is the voltage of the drive, which is the jump before the drive to the plateau during the drive. This now leads to a simple expression which can be used to determine the coupling experimentally:

$$\beta^2 = \frac{\Delta V_{zeppelin}}{V_{drive} Q_{eff}} \tag{2.35}$$

The coupling is a unit less quantity. The coupling plays a big role in the calibration of the experiment's sensitivity. The sensitivity is determined using the square root of coupling β^2 after rewriting equation 2.30. Many other factors come looking into determining the sensitivity. Among these are the the inductance, the spring constant and the properties of the measurement device (SQUID).

The sensitivity has units of [m/V], which can be used to translate the measured voltage back to corresponding amplitude of the motion. The sensitivity is derived in the following way:

$$\frac{V}{r} = \frac{\frac{V}{\Phi_0}}{\frac{I}{\Phi_0}} \frac{I}{r} \tag{2.36}$$

Where $\frac{V}{\Phi_0}$ and $\frac{I}{\Phi_0}$ are properties of the SQUID. $\frac{I}{r}$ is derived from equation 2.30.

$$\sqrt{\beta^2} = \sqrt{\frac{L_{tot} I^2}{k_r r^2}} = I/r \sqrt{\frac{L_{tot}}{k_r}} \tag{2.37}$$

Which can be rewritten into an expression for $\frac{I}{r}$, which can then be used in equation 2.36 for the calculation of the sensitivity.

$$\frac{I}{r} = \sqrt{\beta^2} \sqrt{\frac{k_r}{L_{tot}}} \tag{2.38}$$

2.7 The vibrational modes

In this section previous theory is combined into a derivation on the vibrational modes. There are six degrees of freedom because the levitating particle is not constrained in any dimension. These six degrees of freedom lead to six vibrational modes, these exist out of three translational and three rotational.

Not all modes were calculated to satisfactory results, especially the rotational ones. The problem remains a difficult one. The approximation made the problem easier to interpret. They are however debatable, because we consider a rectangular trap and only one image charge per surface. Higher order image dipoles, images of the image dipoles are not taking into account. The problem has been intensively been studied to the degree that greater understanding of the behaviour of a particle based on its shape and the shape of the trap.

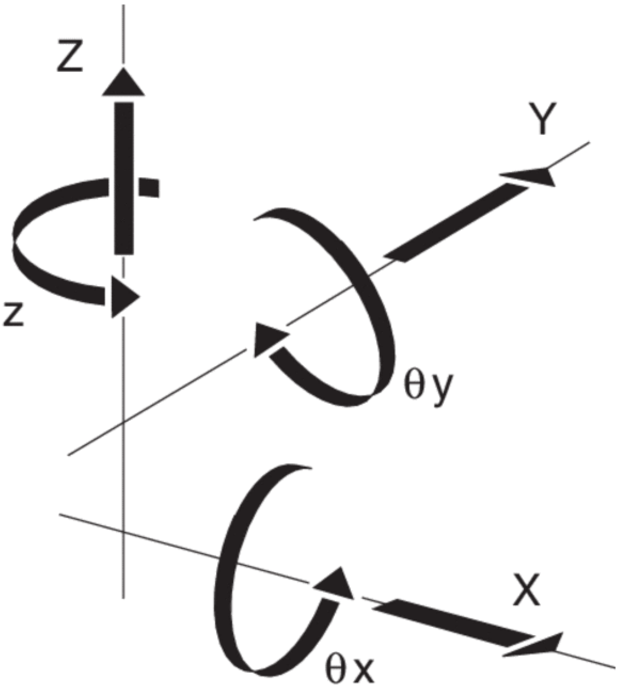

Figure 2.5: *Figure showing the six degrees of freedom consisting from three translational and three rotational.*

2.7.1 Vertical mode: z-mode

The z-mode is the translational mode in the z directions. The z-axis is the axis along which gravity works and can be seen as pointing up with respect to the ground. For the z-mode both the dipole interaction as the pull from gravity are relevant. Therefore both of these potentials are used. Combining these potentials gives:

$$U_{z-mode}(\mathbf{r}) = -\frac{\mu_0}{8\pi}\frac{1}{|\mathbf{r}|^3}[3(\mathbf{m_1}\cdot\hat{\mathbf{r}})(\mathbf{m_2}\cdot\hat{\mathbf{r}}) - \mathbf{m_1}\cdot\mathbf{m_2}] + m_{zep}gz \tag{2.39}$$

Potential

We first need to determine the dot product from the geometry of the problem. A simple approximation of the problem will be used which represents the zeppelin as a simple dipole above an infinite plane, the walls of the trap are ignored. This is shown in figure 2.6 and will be used to determine the dot product in equation 2.39.

Figure 2.39 makes it easy to deduct the dot product using the identity: $\mathbf{a}\cdot\mathbf{b} = |\mathbf{a}||\mathbf{b}|\cos(\theta)$, where θ is the angle between $\mathbf{a}$ and $\mathbf{b}$. This now leads

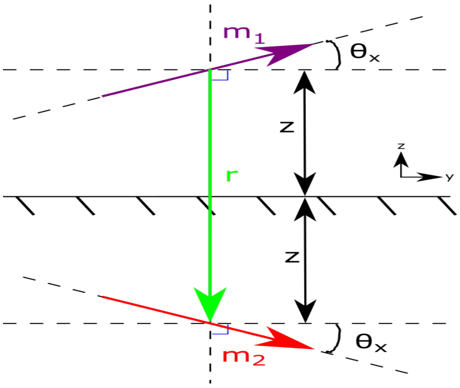

Figure 2.6: *Figure showing the geometric approximation of the problem. Indicating important quantities such as the dipoles* $(\mathbf{m_1}, \mathbf{m_2})$ *and the angle* θ_x*, since this is the rotation around the x-axis.*

to the following dot product for the first term:

$$\mathbf{m_1} \cdot \hat{\mathbf{r}} = m_1 \cos\left(\frac{\pi}{2} + \theta_x\right) \tag{2.40}$$

$$\mathbf{m_2} \cdot \hat{\mathbf{r}} = m_2 \cos\left(\frac{\pi}{2} - \theta_x\right) \tag{2.41}$$

Which can be combined using $\cos\left(\frac{\pi}{2} + x\right) \cos\left(\frac{\pi}{2} - x\right) = -\sin^2(x)$:

$$(\mathbf{m_1} \cdot \hat{\mathbf{r}})(\mathbf{m_2} \cdot \hat{\mathbf{r}}) = -m_1 m_2 \sin^2(\theta_x) \tag{2.42}$$

For the second term the double angle formula: $\cos(2x) = 1 - 2\sin^2(x)$, can be used to rewrite the term in terms of $\sin^2(\theta_x)$.

$$\mathbf{m_1} \cdot \mathbf{m_2} = m_1 m_2 \cos(2\theta_x) = m_1 m_2 (1 - 2\sin^2(\theta_x)) \tag{2.43}$$

The last two equations simplify equation 2.39 to:

$$U_{z-mode}(\mathbf{r}) = \frac{\mu_0}{8\pi} \frac{m_1 m_2}{|\mathbf{r}|^3} [1 + \sin^2(\theta_x))] + m_{zep} g z \tag{2.44}$$

To finalize the derivation $|\mathbf{r}| = 2z$ is used, then we arrive at the final expression:

$$U_{z-mode}(\mathbf{r}) = \frac{\mu_0 m_1 m_2}{64\pi z^3} [1 + \sin^2(\theta_x))] + m_{zep} g z \tag{2.45}$$

Levitation height

The levitation height (z_0) is the height at which the particle will be levitating. This height is the result of the balancing of the gravitational force and the dipole repulsing, as they are accounted for in the potential for the z-mode. The potential needs to be derived with respect to the z-coordinate since this derives the equation from potential energy to force according to $\mathbf{F} = -\nabla U$. θ_x is set to be zero for this derivation since oscillations around this point don't change the height since the magnet is modeled as a single point dipole. For the potential given in equation 2.45 and the z-direction this gives us the following equation:

$$F = -\frac{dU_{zy}}{dz} = \frac{3\mu_0 m_1 m_2}{64\pi z^4} - m_{zep} g = 0 \tag{2.46}$$

Equated to zero since the forces are in balance in the minimum of this potential. Now solving for $z = z_0$ leads to the following expression for the levitation height.

$$z_0 = (\frac{3\mu_0 m_1 m_2}{64\pi m_{mag} g})^{\frac{1}{4}} \tag{2.47}$$

Using the fact that the dipoles are of equal magnitude and $|\mathbf{m_{dip}}| = B_r V/\mu_0$ means that the expression can be rewritten in a form which holds quantities which can be known or estimated. Where V is the volume and B_r the remanence field of the magnet.

$$z_0 = (\frac{3B_r^2 V^2}{64\pi \mu_0 m g})^{\frac{1}{4}} \tag{2.48}$$

Note $m = m_{zep}$, the distinction between the mass and the dipoles is not needed anymore. For the zeppelin discussed in the methods section and used in run28, this results in a z_0 = 0.001862343m = 1.86mm

2.7.2 Lateral modes: x and y-mode

For the lateral modes the problem is slightly different, since here there is confinement due to dipole repulsion from two sides. While for the z-mode the gravity and dipole repulsion balance, here the two dipole repulsions balance. Which is symmetric and therefore the theoretical position of the particle can be said to be in the middle of both lengths. This leads to $x_0 = a_x/2$ and $y_0 = a_y/2$, such that the particle is at (x,y,z)=(x_0, y_0, z_0) if the origin is chosen as of the corners. Note that the values x_0, y_0, z_0 are quite close to each other. Which is worth a point of discussion, when it comes to the infinite plane approximation.

2.7.3 Rotational modes

The rotational modes are the modes of vibrations which are due to oscillating rotations around the x,y and z axis. These are due to the behaviour

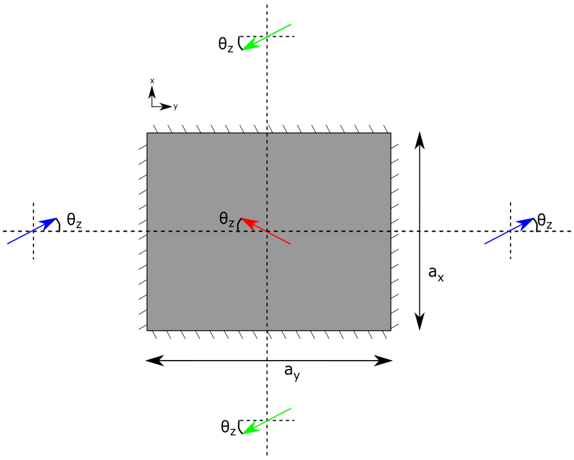

Figure 2.7: Rectangular first order geometric approximation in the xy-plane. Where a_y and a_x are 4.5mm and 3.5mm respectively.

of the potential in the perpendicular plane of the axis around which the rotation happens. A rotation around the z-axis has moving components in x and y, the xy-plane. This would require to set up potentials for the behaviour in these planes, of the form $U_{xy/xz/yz-plane}$. These potentials are more complex to accurately derive even with similar simplification as done before. It is however clear in what way these rotational modes are influenced. As example the θ_z mode can be taken, which is the rotational mode around the z-axis. For this figure 2.7 can be used again. Now four dipoles play a role, furthermore several $\cos(\theta_z)$ and $\sin(\theta_z)$ terms will be present. Although due to the asymmetry of the trap, alignment with the y-axis is expected. In other words $\theta_z = 0$ is expected to be the stable minimum, similar to why θ_x was taken to be zero before. This is why the shape of the trap has been chosen this way, such that the dipole could align in a direction in a stable manner.

2.7.4 Spring constants and frequencies

For these stable minimums the potential can be approximated as a potential of a harmonic oscillator. The potential of a harmonic oscillator is $U_r = \frac{1}{2}k_r r^2$, from which the springconstant, k_r, and the frequency can be derived. For translation modes this is according to:

$$k_r^{trans} = \frac{d^2U_r(\theta_{rr_\perp})}{dr^2}\Big|_{r_0} \tag{2.49}$$

In units of [N/m]. For k_z this can be calculated, using the derived potential.

$$k_z = \frac{d^2U_z(\theta_x = 0)}{dz^2}\Big|_{z_0} = \frac{12\mu_0 m_1 m_2}{64\pi z^5}\Big|_{z_0} = \frac{3B_r^2V^2}{12\pi\mu_0 z_0^5} \tag{2.50}$$

Which leads to a value of $k_z = 3.16 \cdot 10^{-03}$N/m. For rotational modes however the units are bit different, since the movement is a rotation in a plane. Therefore the expressions are slightly different as well:

$$k^{rot}_{\theta_{rr_\perp}} = \frac{d^2 U_{rr}}{d\theta^2_{rr_\perp}}|_{z_0,\theta_0} \tag{2.51}$$

Which is torque in units of [Nm], a difference of m^2 due to not taking a double derivative with respect to distance. Note the use of rr and $rr_\perp$, this is because the potential described in the zy-plane corresponds to the rotation around x which is perpendicular to zy. Next to this here the derivative is done first and then θ_0 is used.

These springconstants determines how the particle oscillates along that direction and at which frequency. Here also two different expressions are handled because the units for the spring constants are different. The difference here is that for the first the mass is sufficient whilst for the latter the moment of inertia, I, must be used rather then the mass of the particle. Interia has units of [kg m^2], this perfectly balances the difference of m^2 in the units. This now leads to the following two expression for the resonance frequencies.

$$f^{trans}_r = \frac{1}{2\pi}\sqrt{\frac{k^{trans}_r}{m}} \tag{2.52}$$

$$f^{rot}_{\theta_{rr_\perp}} = \frac{1}{2\pi}\sqrt{\frac{k^{rot}_{\theta_{rr_\perp}}}{I_{rr_\perp}}} \tag{2.53}$$

For the z-mode this leads to

$$f_z = \frac{1}{2\pi}\sqrt{\frac{k_z}{m}} \tag{2.54}$$

Which returns a value of $f_z = 13.59$ Hz. In practicee runs produce different frequencies then calculated, however the dependencies are known and it gives a rough estimate. This gives insight in to which frequency could belong to which mode, when looking at a spectrum. Furthermore the rough estimate is a good enough answer to see whether the frequencies will be too high or too low with respect to what is roughly needed.

In our experiment the z-mode is lowered by adding non-magnetic mass which lower f_z by increasing m but not increasing k. How this is achieved is shown in the methods section. Experimentally the spring constant for the z-mode is calculated by solving equation 2.54 for k_z, $k_z = m(2\pi f_z)^2 = m\omega_z^2$.

2.8 Sources of dissipation

Sources of dissipation are ways of how energy is lost from the system, through friction for instance. These act as damping factors, they can also be a source of unwanted heating. For these reasons they need to be minimised. In this section the most relevant and dominant factors of dissipation will be briefly discussed. For a more in depth read on these factor I recommend the thesis of Jean-Paul van Soest[7].

Joule heating

One of the more simple, yet stronger sources of dissipation is the process of Joule heating. Joule heating happens in wires when current meets resistance. It is the process that makes old light bulbs glow and also very hot. The power dissipated through Joule heating is given by a simple formula known as the Joule-Lenz law.

$$P = I^2R \tag{2.55}$$

Eddy currents

Eddy currents also form a source of energy loss, since the trap isn't fully superconducting. A thin layer stay normal and this is characterised by the London penetration depth. In this normal layer the resistance is non-zero and thus power is dissipated by the Eddy currents, through Joule heating. Eddy currents are thought to be the main source of dissipation.

Drag

Any object in a medium experiences some form of drag, so does a levitating particle. There are two types of drag, namely form and skin drag. The shape of the object determines how strong each form of drag is. However due to the ultra high vacuum environment the dissipation due to drag will be insignificant. This was shown for a different particle in the calculation in the thesis of Jean-Paul van Soest[7]. It is however safe to assume that the change in particle does not increase the dissipation to a significant amount.

2.9 Aliasing and Spectral leakage

Any signal goes through an analog to digital conversion. When data is converted to digital and subsequently is analysed as such, two effects can occur which influence the data interpretation in a negative way. These two effects are aliasing and spectral leakage. These effect come forth from the fact that a continuous signal is measured and analysed as discrete points in a time. Aliasing is present in the time domain, while spectral leakage becomes mainly apparent in the frequency domain after a Fourier transform has been done. Here seemingly new and different frequencies then the signal's frequencies occur.

2.9.1 Aliasing

Aliasing is an effect that occurs when the signal which is measured is of way higher frequency then the frequency with which data point are acquired. This leads to a loss of information, where the data points don't represent the actual signal well enough. This generally causes wrong interpretations of the data points.

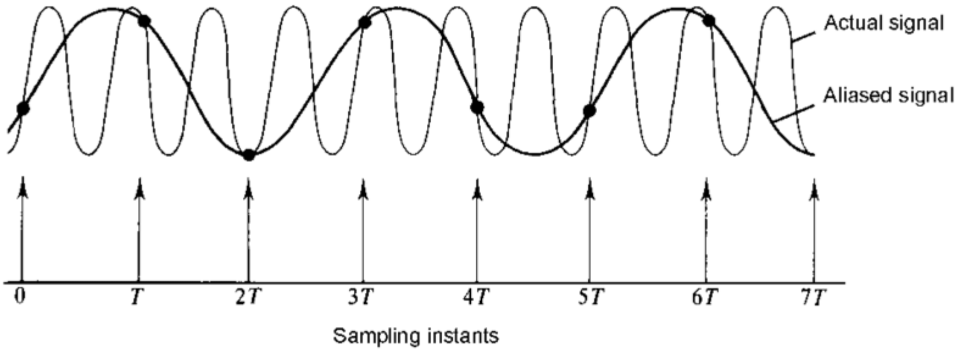

Figure 2.8: *A simple example of aliasing can lead to a wrong interpretation of data points.*[8]

Aliasing can be prevented by taking a high enough sample rate to prevent the loss of information, furthermore the use of a low-pass filter to prevent any unwanted high frequency signals to enter the data is also highly effective. In our research a sample rate of 3.5135 sample/second is used and the lock-in has a programmable low-pass filter, which was in general set to Tc = 2s.

2.9.2 Spectral leakage

Spectral leakage is the effect where other frequencies then the signal's frequencies occur in the Fourier transform of the signal. This is called spectral leakage and the name comes from the idea that energy of the correct frequencies leaks into the surrounding frequencies. One of the main reasons for spectral leakage is windowing, especially when it breaks the periodic continuation of the signal.

Windowing is the action of taking a discrete time interval of a continuous signal. The most simple and the one applied in our research. These windows have a non-zero Fourier transform, which becomes convoluted with the transform of the continuous signal producing spectrum which is leaking. A rectangular window has a sinc function as its transform, in continuous transforms this will always be visible.

However digital data is discrete and therefore discrete Fourier transforms (DFT) are used, this changes things. Since for a DFT if the periodic continuation of the signal is preserved the zeros of the DFT coincide with the zeros of the since function, producing no non-zero values where they do not belong. Spectral leakage can thus be minimised and/or prevented by two actions. The usage of different windowing function, who's Fourier transform has a different shape. Or by making sure that the signal's periodic continuation is not violated. The latter of the two methods was implemented in the data analysis, no other window then a rectangular window has been used. This because a rectangular window has the best frequency resolution.

Examples

Spectral leakage is best shown using figures as an example. As starting point a sinus with a frequency of two and amplitude of one is taken, in a time interval [0,10) in seconds. After which the signal is cut off from both the left and right, in such a manner that the amplitudes do not match. This means the curve becomes non periodic. The DFT that was used is numpy.fft.fft which is an Fast Fourier Transform (FFT).

Periodic example

The figure below shows the starting point, an unaltered and periodic sine function and its FFT.

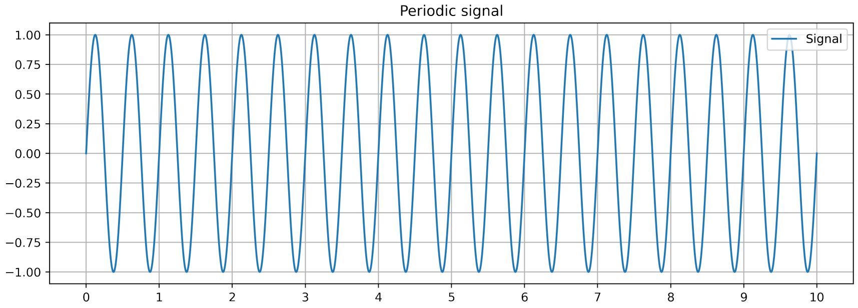

(a)

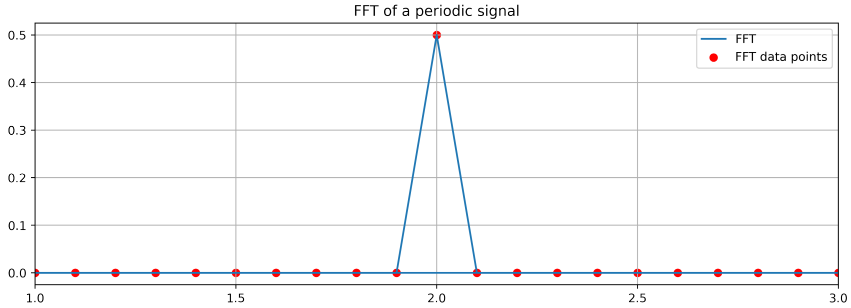

(b)

Figure 2.9: ***(a)*** *A signal whose periodic continuation holds, which then produces a transform* ***(b)****. Here the discrete points are indicated in red, showing how they clearly are all zeros apart from the true frequency of the signal.*

Non-periodic example

After altering the signal the same bit of code produces the figures below, showing how the same sine function in a different time interval produces a distinctly different FFT.

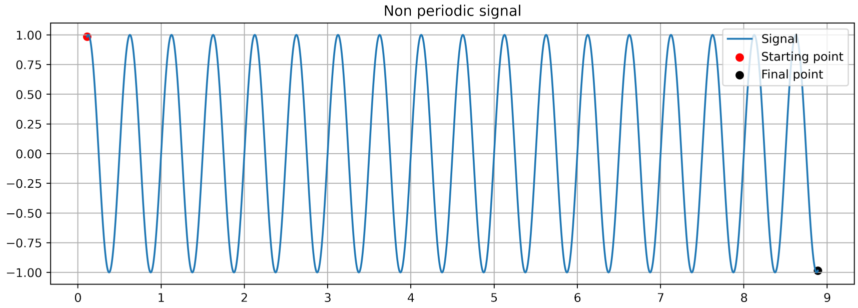

(a)

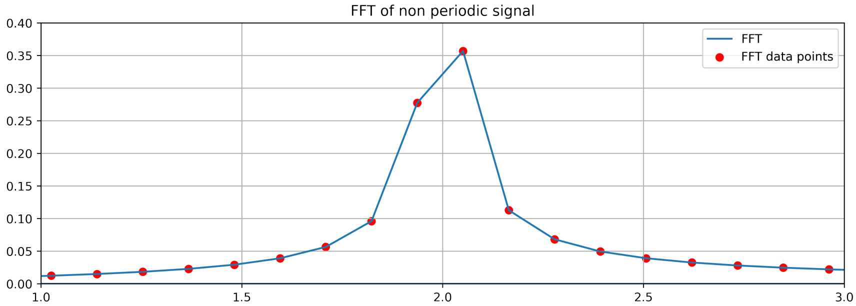

(b)

Figure 2.10: *Signal* ***(a)*** *now is non periodic, chosen in such a way that the amplitudes of the indicated starting and ending point are relatively far apart. This creates a relatively big step function which should produce spectral leakage. Looking at the transform* ***(b)*** *the spectral leakage is clearly visible. Non zero values apart from the real frequency and two data point of similar height fall next to two but not one signal on two like before.*

2.10 Frequency resolution

To be able to see a sharp signal and distinct signal, a sufficient frequency resolution is needed. A smaller df means better frequency resolution.

$$df = \frac{1}{\Delta t} = \frac{f_{sample}}{N_{samples}} = f_{i+1} - f_i \tag{2.56}$$

Since $N_{samples} = f_{sample} \cdot \Delta t$ thus $\Delta t = \frac{N_{samples}}{f_{sample}}$. Where the sample rate (f_{sample}) and number of samples ($N_{samples}$) are relevant.

Again a reason to have a high enough sample rate, however next to this it becomes clear that sampling for a longer time (Δt) results in greater frequency resolution. This can be confirmed by checking the difference between to neighbouring frequencies (f_{i+1}, f_i) value's on the frequency axis of an DFT.

Chapter 3

Methods

Theory leads to practice. In this chapter the discussed theory will be put in to practice. Showing the used methods of how the low temperature, low pressure and low vibrations were achieved. Furthermore showing the experiment itself, its vital parts such as the trap and the magnet, and how measurements were made.

3.1 Controlled environment

Due to the sensitive nature of the experiment a controlled environment with low temperature, low pressure and low vibrations is a must. This section will elaborate on why this is a necessity and how this is achieved.

3.1.1 Cooling

Cooling plays a vital role in the experiment, this is because of several factors. One of the most evident is the fact that a low temperature type-I superconductor is used as a trap, which requires cryogenic temperatures to be superconducting. Furthermore cooling reduces temperature dependent noise. Cooling is achieved using a cryostat from Leiden cryogenics, known as a dry dilution refrigerator.

Version of July 4, 2022– Created July 4, 2022 - 18:59

Dry dilution refrigerator

A dry dilution refrigerator has the ability to reach miliKelvin temperatures. This is achieved using several liquid gasses, these are: Nitrogen, regular helium-4 (^{4}He) and an isotope helium-3 (^{3}He). Nitrogen is used as a relatively cheap pre-cooling method, since ^{4}He and especially ^{3}He are more expensive, liquid nitrogen has a boiling point of 77K. Next liquid ^{4}He will be used to cool down further, it has a boiling point of 4K. ^{4}He is used in combination with pulse-tube (PT), the PT pumps the ^{4}He through the cryostat in a closed cycle. The PT is what makes this a dry dilution refrigerator compared to the normal wet dilution refrigerator. Since the PT replaces the cooling baths normally present in a wet dilution refrigerator, hence the name dry.

During the cycles of the pulse-tube the ^{4}He is compressed and decompressed. This is a thermodynamic process in which energy is taken away from the ^{4}He. The decompressed ^{4}He is then cycles back in the cryostat, the PT has a frequency of 1.4 Hz which is noticeable via the SQUID and one of the main reasons for improving vibration isolation inside the cryostat. The PT is connected to the first two plates in the Outer Vacuum Chamber (OVC), these two plates are the 50K and the 4K-plate. This however still does not get us the miliKelvin temperatures, these are achieved through the dilution of the ^{4}He with ^{3}He.

This dilution happens in what is known as the mixing chamber, which is a closed system in the Inner Vacuum Chamber (IVC). In the mixing chamber ^{4}He is also present and is now mixed with ^{3}He. In the mixing chamber now two phases of are separated, these are known as the concentrated and dilute phase. The dilute phase is a mixture of roughly 6% ^{3}He and 94% ^{4}He, whilst the concentrated phase is almost 100% ^{3}He. The concentrated phase lies on top of the diluted phase, separated by a phase boundary. ^{3}He dilutes from the concentrated phase through the phase boundary into the diluted phase. This process removes energy from the surroundings. The ^{3}He evaporates and is cycled back into the system later on, repeating the process. This cycle keeps removing energy and thus heat from the system in this way providing cooling power.

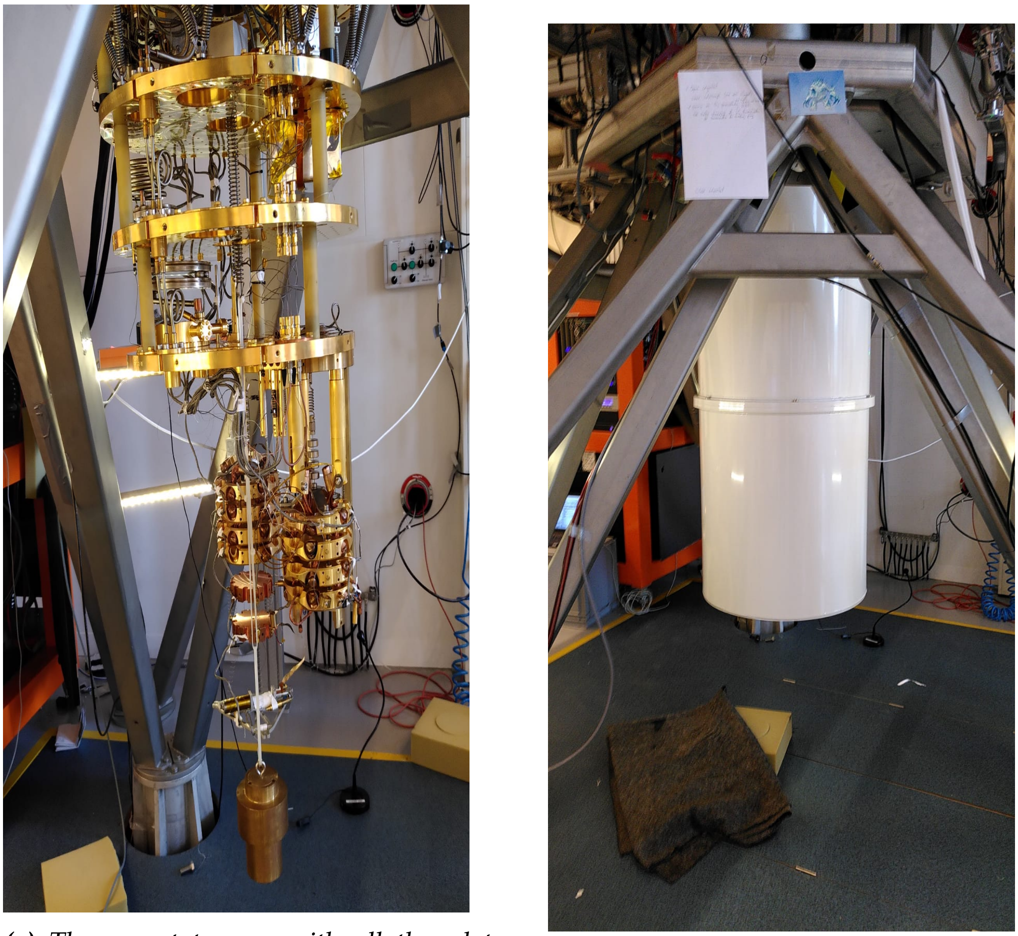

(a) *The cryostat open with all the plates, masses and springs clearly visible.*

(b) *Crystat closed, also showing its double tripod suspension.*

Figure 3.1: *Two pictures of the cryostat in open and closed state, in later stadium of my internship. Showing several component which will be discussed in the rest of the method section.*

Thermal conductance

Since there is a vacuum present there is little medium through which heat can be extracted from the experiment. To ensure cooling reaches the experiment silver ribbons are used as a means to conduct heat. A silver ribbon is connected to the mixing chamber plate, since this is the plate best cooled, and reaches all the way down to the housing of the experiment. This is shown in figure 3.2, with two pictures which demonstrate the attachment of the silver ribbon. The silver ribbon is made sure to have a firm connection to the masses to ensure the best possible thermal connection. Furthermore this good connection to the masses and the bends in the silver ribbon need to make sure that the ribbon doesn't form a bypass for vibrations.

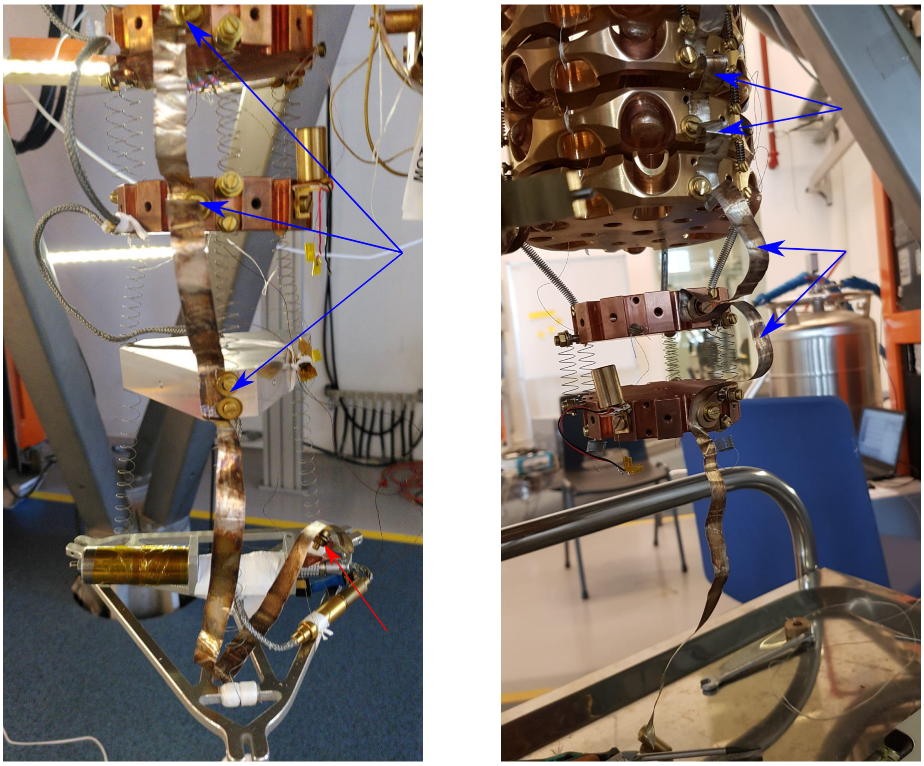

(a) *Picture showing the lower part of the vibration isolation system and how the silver ribbon is connected to the masses (blue) and eventually to the experiment (red).*

(b) *Showing the upper part of the vibration isolation system, showing the bends in the silver ribbon (blue). These bends minimise the involvement in connecting the masses mechanically.*

Figure 3.2: *Two pictures of how the silver ribbon is attached to all the masses, all the way down to the experiment.*

3.1.2 Vacuum

A vacuum is needed to be able to achieve a gravity measurement because gravity is so weak. Too large a pressure would contribute to too much drag on the particle, which would dominate over gravity. Making it impossible to measure gravity through all the drag noise. Therefore it is important to decrease the pressure to such a level that the drag is reduced to a insignificant level of damping. A vacuum is achieved in both the OVC and the IVC, the vacuum in the IVC is considered a ultra high vacuum. The vacuum is achieved through the use of several pumps. This process starts with the use of a giant pump, which is great for the big volume at first. After which more specialised pumps, such as a turbo pump, are used to achieve the higher vacuum. Finally, when the system is cold all the walls act as extremely effective cryopumps and the pressure can no longer be measured.

3.2 Vibration isolation

Any motion of the setup would influence the flux, since the pick-up coil moves relative to the zeppelin, and thus the measurement. Therefore inhibiting these motions is of great importance to do good measurements which are as undisturbed as possible. Since a SQUID is capable of measuring with great sensitivity and the small motions of the zeppelin, the vibration isolation must be extremely good or else only vibrations would be visibly measured. Our aim is to build a gravity force sensor, not a vibration force sensor.

The cryostat is isolated from its surroundings on what is known as a measurement island. The cryostat it is hanging from a giant tripod which stands on a measurement island, as can be seen in figure 3.1b. This hinders vibrations created in the direct surrounding of the cryostat. There are two tripods, an outer one standing on the floor of the lab and an inner one which is connected to the measurement island. The outer one carries several machines which can produce vibrations, such as the pulsetube, but are still need close to the top of the cryostat.

This measurement island exist of a 25 ton block of concrete which rests on dampers. However this isn't nearly enough, vibrations of substantial strength can still reach the cryostat, especially those of the equipment above the cryostat of which the pulse-tube is the primary source. Therefore there is also a lot of vibration isolation present inside the cryostat. The systems present here are dampers, springs and masses. These are present in between the plates and a giant several stages mass spring system is used to isolate the experiment even more from the rest of the cryostat.

This system can be seen in figure 3.3a, which shows the version of the vibration isolation which was used in run28 after developing it for several runs.

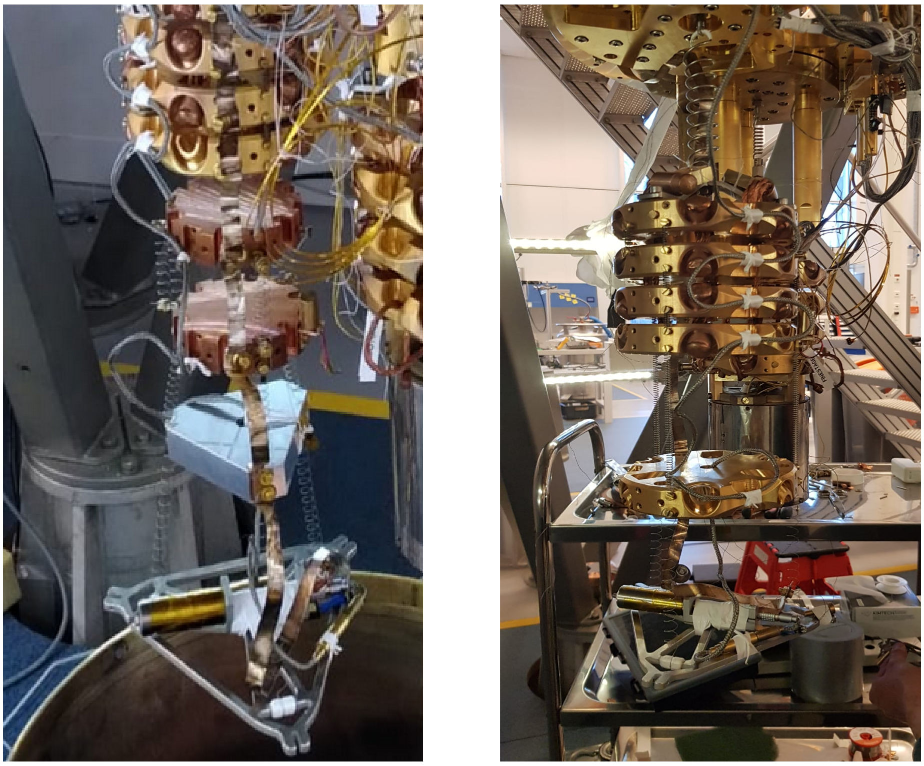

(a) *The more recent vibration isolation. Which consisted of more lighter masses, this allowed for adding more springs.*

(b) *An older version of the vibration isolation. Less stages and here it is hanging from the mixing chamber plate.*

Figure 3.3: *Two pictures of two moments in the development of the vibration isolation.*

This development mainly consisted of adding more masses and soft springs up to the point that the vertical space was used up. This can be seen in comparison to an earlier version which is visible in figure 3.3b. One of the biggest developments on the vibrations isolation, was a giant soft spring. Which hangs from a suspension on one of the higher plates all the way down through the holes in the plate to the system of masses and springs as seen in figure 3.1a

3.3 Measuring

Measurements are performed with a SQUID, which stand for Superconducting Quantum Interference Device. This is a device capable of measuring extremely small magnetic fields. It achieves this by measuring quanta of flux through the use of Josephson junctions. A flux quantum equals: $\Phi_0 = \frac{h}{2e} \approx 2 \cdot 10^{-15}\ Tm^2$. Next to this their noise level is extremely low, $\frac{m\Phi_0}{\sqrt{Hz}}$ as well. Exactly these reasons make SQUIDs perfect for measuring a force as weak as gravity. The SQUID is read out with a Zurich Instrument (ZI) lock-in amplifier, hooked up with a 10MHz atom clock.

The SQUID used for the experiment is is the following:
Magnicon all in one, CAR in NC. L S0008:NC, C648_K22:CAR, 400 nH.

CAR is the carrier chip, NC stands for Niobium Can (shielding) and L stand for size L SQUID. This L sized SQUID has two properties which are important for the calibration: $\frac{V}{\Phi_0} = 0.43\ \frac{V}{\Phi_0}$ and $\frac{I}{\Phi_0} = 0.5\ \frac{mA}{\Phi_0}$, these are found in the manual for the SQUID.

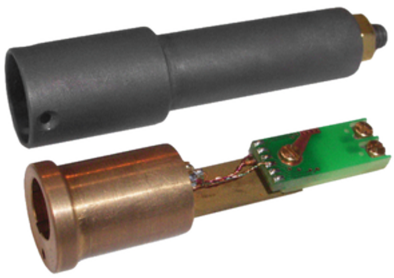

Figure 3.4: A picture showing a SQUID with the carrier chip (green chip in bottom item) and the niobium shielding (top item).[9]

3.4 Experimental setup

Whilst the cryostat and many things around the experiment are rather big, the heart of the experiment is actually quite small. This is the experiment and it's housing. All the vibration isolation present is to minimise the vibrations on this object. It is on the lowest platform of the cryostat. We try to use every centimeter here, to be able to put as much vibration isolation in between as possible. The housing containing the experiment has an important function next to holding everything in place. It also shields the experiment and the SQUID from outside flux, which could interfere with the measurements.

3.4.1 Trap

The trap used is an elliptical cylinder made of tantalum. On this trap a lid can be put to close it off. The lid contains holes for the wiring of the pick-up coil and for air to escape to establish a vacuum.

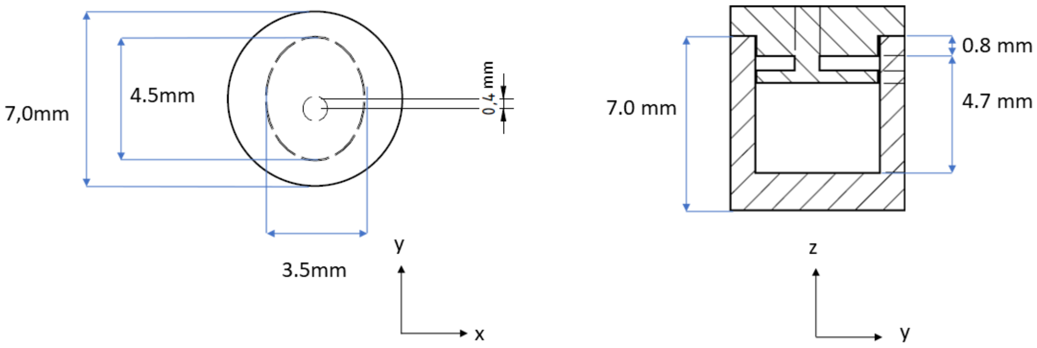

Figure 3.5: *Schematic of Lake Ontario as designed by the FMD, figure adapted from the thesis of Dennis Uitenbroek.*[10]

The elliptical shape was chosen to break the symmetry in the xy-plane, such that the dipole moment of the zeppelin would align with the y-axis. The trap is held in place by a slightly bigger hole in an aluminium housing. This and the lid that covers the trap can be seen in figure 3.6a. Next to this in figure 3.6b is the pick-up coil, which is used to pick-up the flux of the zeppelin and also used for the magnetic drive. The elliptical shape of the trap can be seen in figure 3.7a. The trap was just cleaned through the process of etching with chemicals. This makes sure no sticky oxides are inside the trap. These oxides are non-superconducting and could pose a

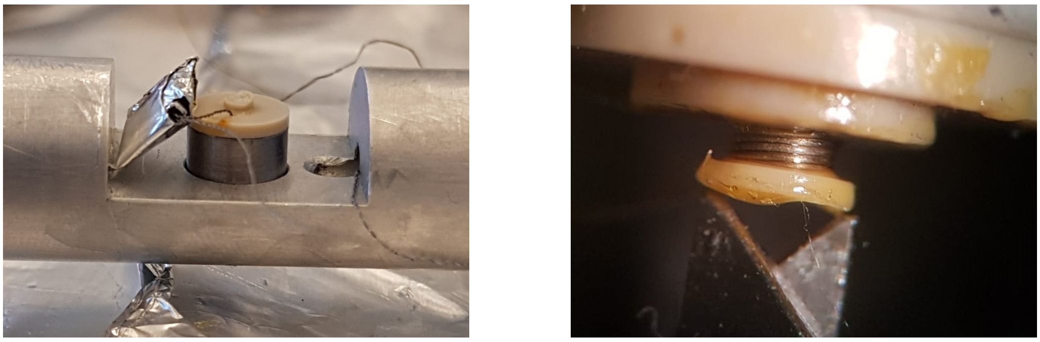

(a) *The trap inside its own confinement with the aluminium housing. Seen here as well are the lid of the trap and the wiring including the in aluminium foil wrapped transformer.*

(b) *Picture taken from the bottom side of the lid, whilst it was under a microscope during fabrication of the pick-up coil. Here 2 of the 4 layers of 5 turns of roughly 0.8mm were made.*

Figure 3.6: *Two pictures showing the trap and transformer.*

problem for lift off of the zeppelin. Alos, they might be responsible for dangling bonds that cause damping at low temperatures.

For this same reasons tantalum has been chosen since it forms oxides less quick than the previously used lead and remains a type-I superconductor. Furthermore tantalum has similar critical values as lead, its values are: $T_c = 4.48$ K, $B_c = 0.09$ T. Compared to those of lead: $T_c = 7.19$ K, $B_c = 0.08$ T, where the 3 K difference in T_C is irrelevant, since much lower temperatures are reached.

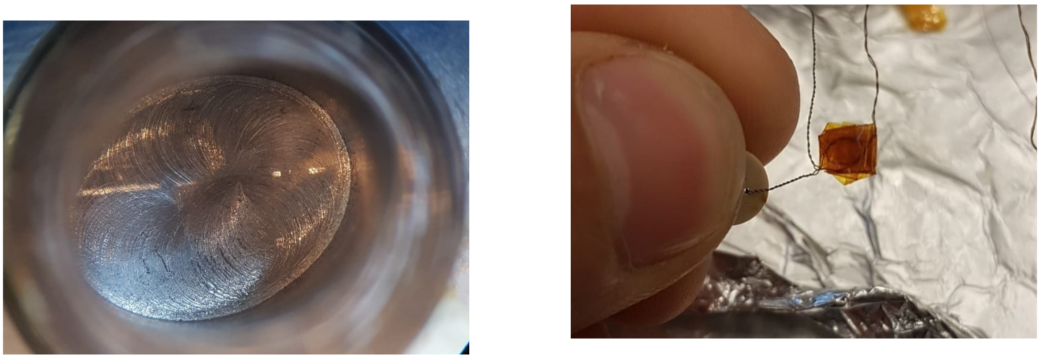

(a) *Trap as seen from above through a microscope, just after cleaning it. Showing the elliptical shape and the clean bottom.*

(b) *Showing the transformer before it was wrapped into aluminium foil. The overlaying 1:1 loops are visible and how they are integrated with in the twisted pair wires.*

Figure 3.7: *Two pictures showing parts of the circuit and housing/confinement.*

3.4.2 Housing and shielding

To shield the experiment there are two primary shields. One is cylinder-like shaped tube with one open and one closed end, which can be put over the aluminium (Al) part which holds the trap. The other is a Niobium (Nb) casing in which the SQUID operates, Nb has a high critical field of 0.82 T and this makes it a great shield. Nearly the complete housing becomes superconducting and thus shielding. Since both Nb and Al are superconductors, type-II and type-I respectively.

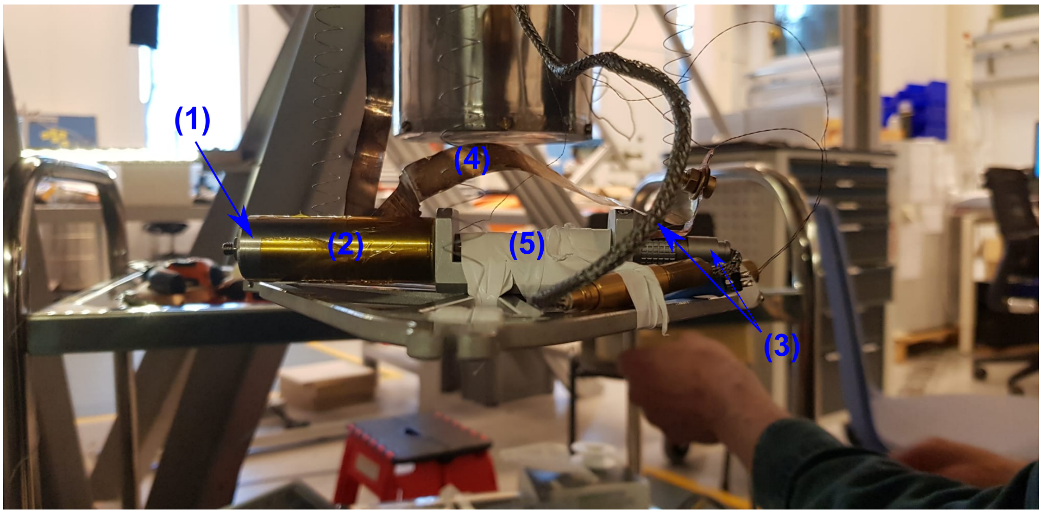

Figure 3.8: *Picture of the lower platform containing the experiment. Several parts are indicated: (1) Shielding of the trap. (2) Location of the trap within the shielding. (3) SQUID cable. (4) Thermalisation. (5) Location of the SQUID with in the Niobium shielding.*

The housing rests upon a triangular aluminium frame. This is located at the bottom of the systems of mass and springs, being the last system. This bottom frame is quite light and hangs on soft springs, therefore considering the weight of the housing and even that of the thick SQUID cable a fine balance had to be found such that the frame would be as water level as possible. Else the trap and such the experiment would be angled too much with respect to gravity. Everything is kept in place by nylon tape, which is visible as the white straps in figure 3.8.

3.4.3 Circuit and wiring

All the different electrical components need to be connected in the correct way. The main components are the SQUID, the pick-up coil, the calibration transformer and the Lock-In. A simple schematic is shown in figure 3.9.

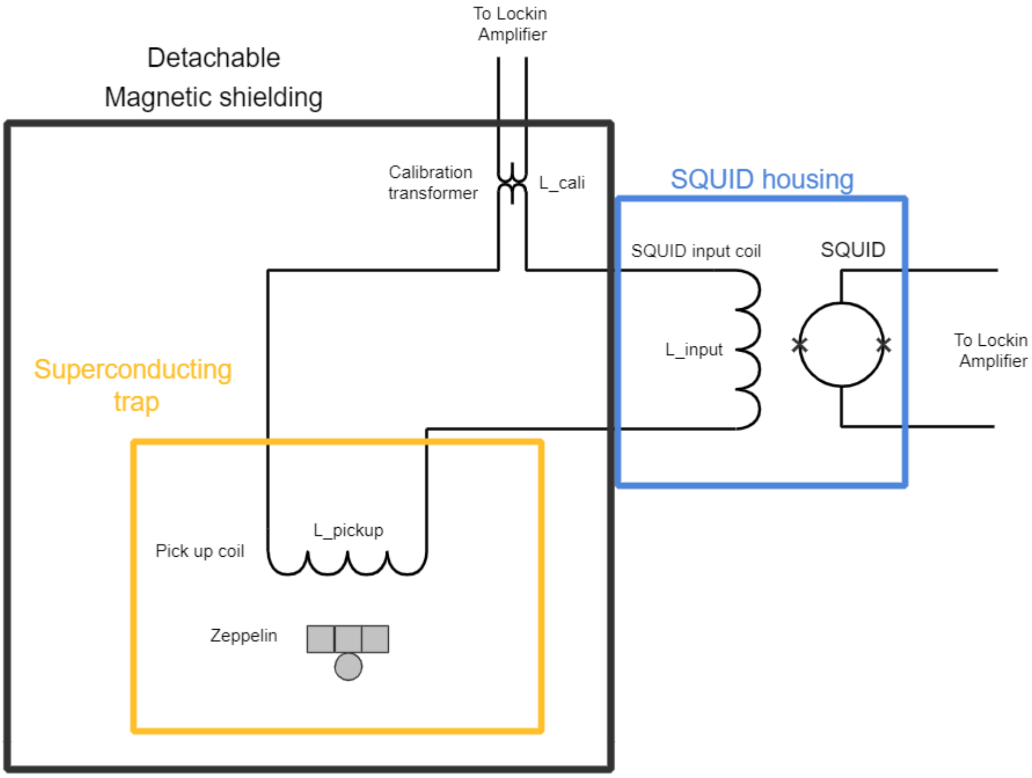

Figure 3.9: *Schematic of the wiring and components of the experimental setup.*

The wiring is for the most part twisted and consists of superconducting wires. In these twisted pairs the wires running in opposite directions have opposing magnetic fields, which will nullify each other. This is especially important for the wires close to the experiment, for logical reasons of interference. In several figures the twisting of wires is visible, it is especially visible in figure 3.7b where the calibration transformer is shown.

3.4.4 Zeppelin

The particle and thus resonator in question, is what we call the zeppelin. Named after the lead zeppelin. It can be seen in figure 3.10, where a photo (3.10a) and a schematic (3.10b) of the zeppelin are shown.

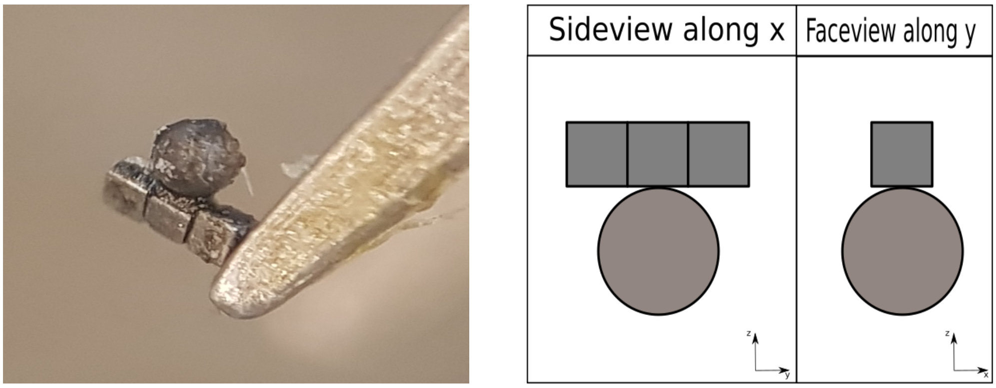

(a) The zeppelin used in run28 seen under a microscope, on the tip of a tweezer.

(b) Schematic model of the zeppelin used in run28. Same axis as the trap.

Figure 3.10: *Two figures displaying what kind of particle was used, consisting of three small cubic magnets and a glass ball.*

As shown the zeppelin consist of several smaller parts, these are three cubic magnets and a small glass ball. The cubic magnets are micro-magnets which have sides of 0.25mm, and where imported from supermagnetman.[11] Three of these magnets aligned as shown thus form a magnet of 0.75mm x 0.25mm x 0.25mm. The magnets are N50 Rare Earth Neodymium (NdFeB) magnets with a nickel-copper-nickel coating of 12-25 μm. They are of N50 grade and this corresponds with a remnant magnetic field known as B_r of 1.39 to 1.44 Tesla.[12]

The glass ball is an addition which was made to add some non-magnetic mass, this mass would not contribute to the repulsive forces at play. It would add mass and inertia. This is done to influence the modes in such a way that these would be separated better and that the frequencies would be lower. These dimensions for the different densities makes it possible to get an estimate for the mass. The mass of this zeppelin has been estimated at $m = 4.3 \cdot 10^{-7}$ kg $= 0.43$mg.

3.5 mass wheel

To measure gravity in a controlled and confirm-able manner, a gravity wheel is used. This wheel has three masses attached to it and can be spun up to a certain angular speed. This speed will correspond with a certain frequency. To measure this frequency a laser and a photodiode are used.

The mass wheel is kept at the correct frequency, in lock, by a proportional feedback based on the signal of the laser. The frequency of the wheel is set at a slight off set compared to the mode on which a gravitational measurement is done. Why this is done will be made clear in the results. A picture of the mass wheel in question can be seen in figure 3.12 together with the bridge on which the wheel is mounted.

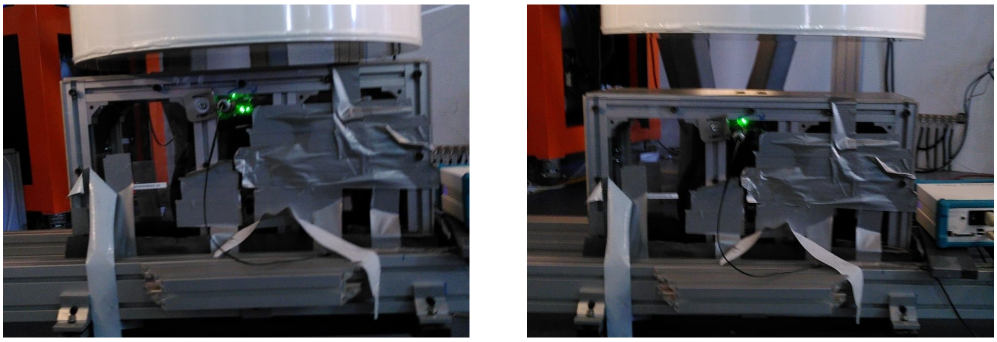

(a) *Higher position of the wheel(N).* ***(b)*** *Lower position of the wheel (N-5).*

Figure 3.11: *The mass wheel on two different height positions on what was known as the lateral position: pos5. The laser can be seen as well by the little green light.*

This wheel was moved laterally and vertically whilst it is fixed on a bridge. This bridge sat on several planks and those again on a trolley, allowing for vertical and lateral movement. The bridge and the strapped on mass wheel can be seen in the pictures of figure 3.11, here the vertically displacement is shown. The vertical displacement was achieved by altering the number of planks on the sides of the bridge. These planks have a thickness of 18mm, in total a max displacement of 6 planks (10.8cm) was done in the following steps: N,N-5,N-3,N-1,N+1, where N is the original height consisting of N planks.

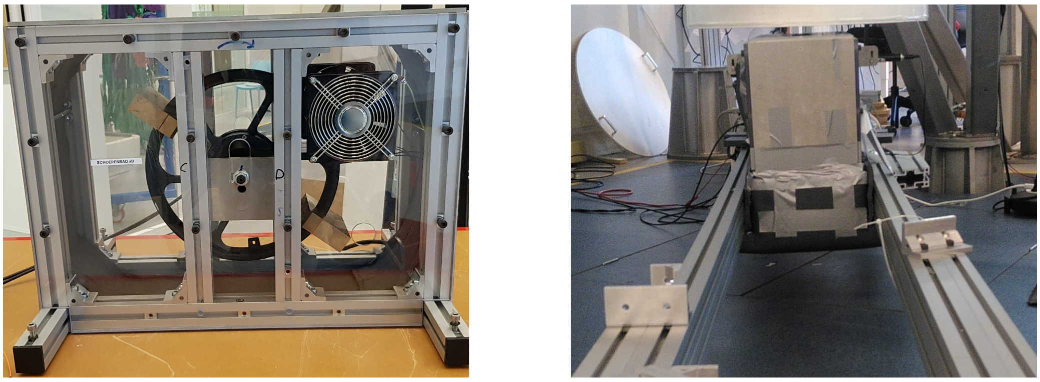

(a) *Picture of the mass wheel used to induce a fluctuation in the local gravity of the zeppelin. The picture is adapted from the thesis of Dennis Uitenbroek and shows the mass wheel with two mass compared to the current three.*

(b) *The bridge on which the mass wheel was placed, the bridge stretched completely over the wooden floor beneath the cryostat. This was to prevent any vibrations which the mass wheel produced from traveling to the cryostat.*

Figure 3.12

3.5.1 Effects of the mass wheel

The mass wheel has been put into different position, these different positions due to different displacements have different effect. This section shows why and how the amplitude and phase behaviour change depending on the position of the wheel.

Positional effects

The amplitude and phase of the signal change with displacement of the mass wheel. The amplitude change is easy to understand since gravity drops off with distance. If the displacement increases or decreases the distance then amplitude of the signal decreases of increases respectively. The change in the phase however is well demonstrated by figure 3.13. The same mass points towards the zeppelin for a different angle. Here obviously the distance increases as well, so the phase and the amplitude both change. For vertical displacement roughly underneath the cryostat the amplitude will change but the phase hardly.

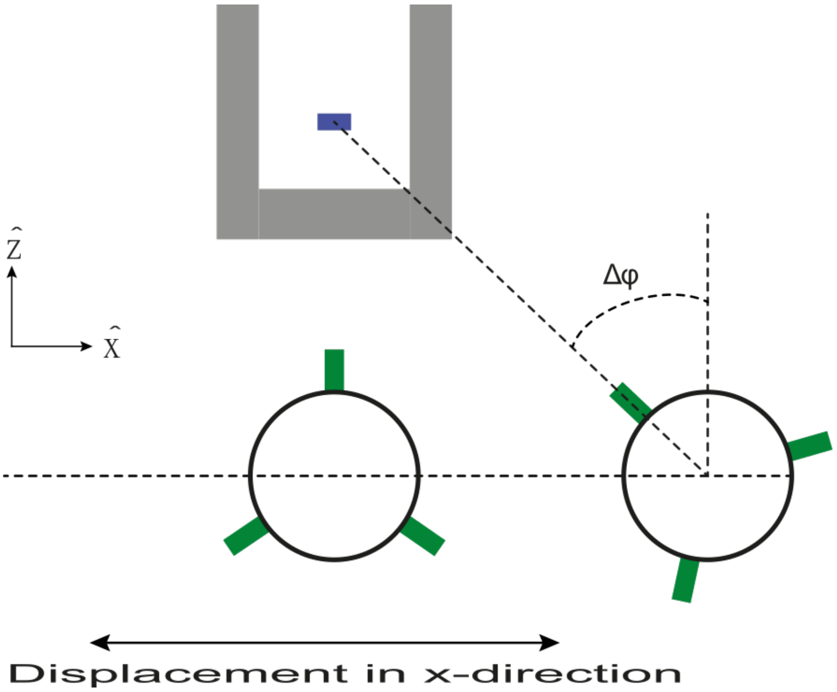

Figure 3.13: *A schematic drawing showing how the phase of the gravitational interaction shift with the lateral movement of the mass wheel. Image adapted and altered from the thesis of Dennis Uitenbroek.*[10]

3.5.2 Simulations

Simulations have been performed based on the previous work of Dennis, several variables are changed or introduced. The original one point mass was replaced by a grid of 4 times 6 24 point masses.

This was done to account for the finite size of the mass, which is on centimeter scale. This scale is of the scale at which the displacements are, thus making it relevant. Next to this the small fluctuations of the wheel are taken into account, the mass wheel doesn't stay on frequency perfectly. Any influences on an other frequency decrease the addition to the correct one, this is taken into account as a factor of $\cos(\text{fluctuations}) \approx 0.97$ for the simulation. Furthermore the results are calculated as Root Mean Square (RMS) values, since the signal voltage is thought to be a RMS value.

Figure 3.14, shows the results from Dennis his simulations. They are here for reference and to show the difference compared to the new simulations. On top of this, the new simulations were only done for the z-mode. The simulations of Dennis can be used as supporting argument when considering the shape of the x- and y-mode. Since these are not rule out yet.

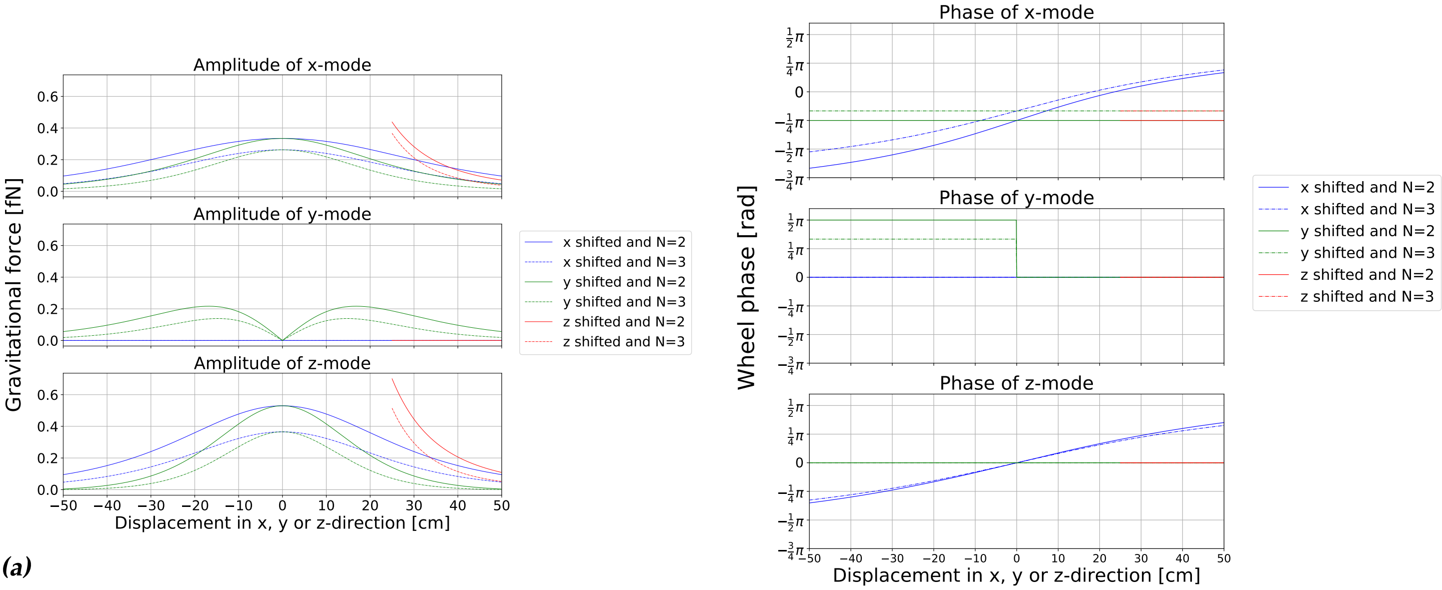

(a)

(b)

Figure 3.14: *Several simulations are shown for the different lateral modes. These consist of* ***(a)*** *the simulations for the amplitude and* ***(b)*** *the simulations for the phase. These simulations were done by Dennis Uitenbroek.*[10]

Vertical simulation: z-mode

From the vertical simulations two plots are produced, these are visible in figures 3.15 and 3.16. Showing both the amplitude and phase behaviour depending on the lateral displacement. The amplitude figure shows several dotted curves that illustrate how the force varies with later displacement, of which the even line is an average.

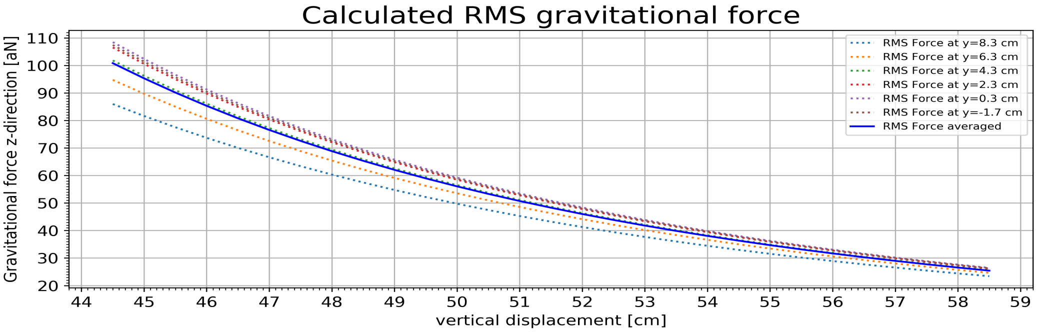

Figure 3.15: *Simulation based on the work of Dennis Uitenbroek done by Tjerk Oosterkamp. Simulating the expected gravitational force of the mass wheel on the zeppelin, based on complex numbers. The x-axis is displacement in x and the different curves are for different displacements in y, an average of the curves is included.*

The figure on the phase shows a clear linear plot where the origin is crossed. This line is based on the average line of the previous plot. These two plots are our expected benchmark for the results.

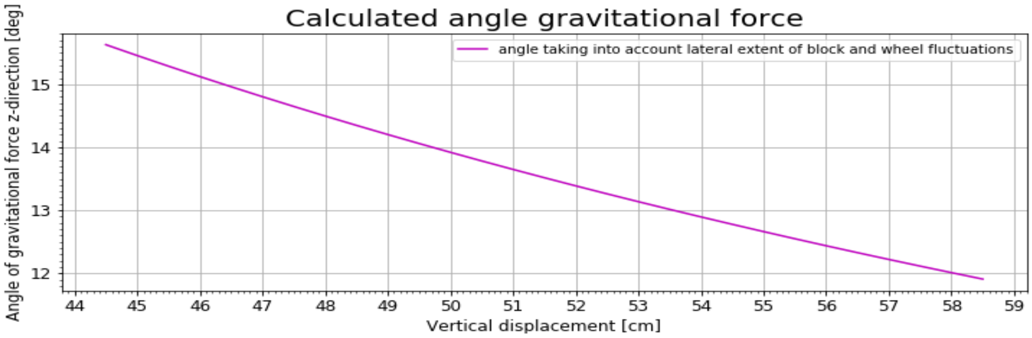

Figure 3.16: *The corresponding phase simulation for vertical displacement. The change is is just a matter of several degrees.*

Lateral simulation: z-mode

In similar fashion a simulation has been done for lateral displacement. These are shown in the figures below.

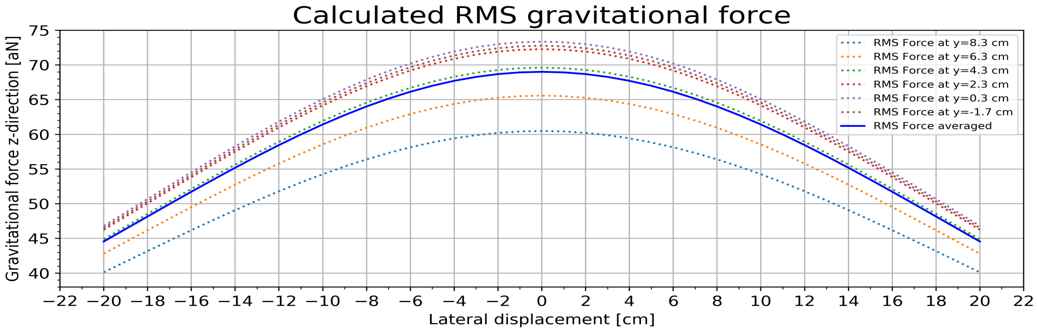

Figure 3.17: *Results of a simulation for the expected RMS force for lateral displacement of the mass wheel.*

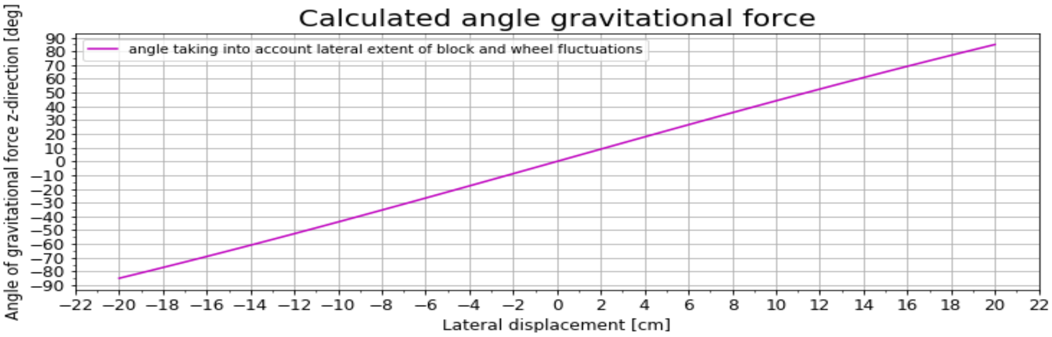

Figure 3.18: *Phase simulation for lateral displacement of the mass wheel. This figure clearly shows the huge impact lateral displacement has on the phase.*

Chapter 4

Results

In this section the results of run 28 will be presented as follows:
1) The achieved spectrum of run 28.
2) The characterisation and calibration of the 26 Hz mode.
3) Gravitational measurement:
  3a) Analysis on one data point.
  3b) Analysis on the collective of the data points.
Extra plots are added in the appendix, under appendix B.

4.1 Spectrum of run28

At the start of each run the first thing which is looked at is the spectrum of the SQUID signal. This gives a broad image of the frequency response of the experiment, hopefully clearly showing eigenmodes of vibration and their amplitude. The spectrum is shown in figure 4.1 and 4.2, this was the results of 65 averages and was a clean and clear spectrum. The spectrum shows distinct peaks which pop up above the noise level quite well. These peaks are eigenmodes of vibrations measured by the SQUID.

The spectrum shows several things. One of which is that is it quite busy and noisy in the lower frequency range below 10 Hz. This has to do with the vibration isolation which act as low pass filters and are better at reflecting higher frequencies. In this range also the resonances of the vibration isolation can be found. This is show better in figure 4.2 in the orange area, these peaks also tend to be broader. Another thing which is important to note is that the peaks an integer number times 50 Hz are the 50 Hz of the electrical net and it's higher harmonics, these are not eigenmodes of the zeppelin and are ignored. With six eigenmodes to find and not too many peaks of which several not relevant, it looked rather promising and it turned out to be. In relatively quick succession in comparison to previous runs all six modes were found through magnetic drive at the peaks in the spectrum. The modes of the zeppelin have roughly the following frequencies and are named as such: 15 Hz, 26 Hz, 40 Hz, 55 Hz, 129 Hz and 146 Hz. Of these the 26 Hz mode was suspected to be the vertical mode on which we wanted to use the mass wheel and look for gravitational signals. These modes can be characterised and calibrated, this especially important for the 26 Hz mode.

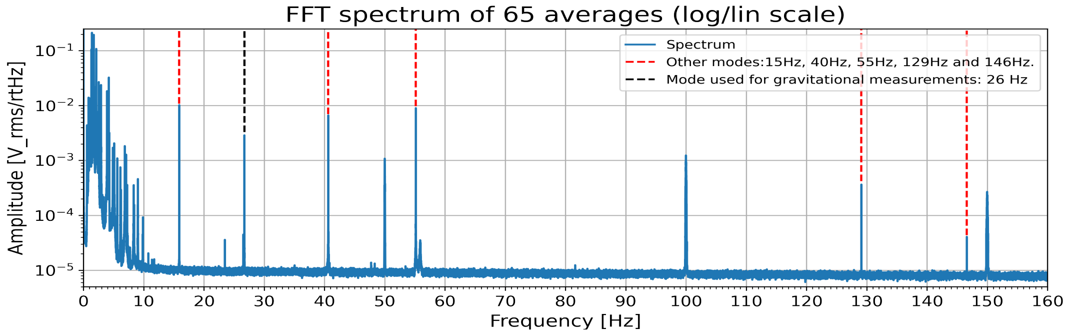

Figure 4.1: *Spectrum of 65 averages taken of run28 in log/lin scale, plotted between 0 and 160 Hz. The most important mode, the 26 Hz mode has been indicated by the black dotted line, while the other modes are indicated by the red line.*

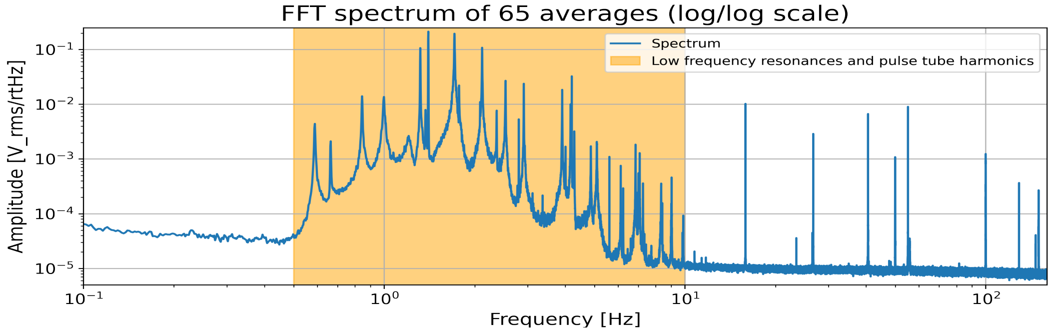

Figure 4.2: *The same spectrum of run28 in log/log scale, in this way clearly showing the several low frequency resonances. These are hypothesised to be low frequency resonances of the vibration isolation and pulse tube harmonics ($N \cdot 1.4Hz$).*

4.2 Charaterisation and calibration of the 26 Hz mode

This sections shows two measurement on the 26 Hz mode:
1. How the tau of the mode is determined from a ringdown, which is also a measure for the Q-factor of that mode.
2. How the coupling of the mode is determined using the magnetic drive.

The methods used in the ringdown measurement are also of used for the data analysis on the gravitational measurement. The coupling is the calibration part. The same types of measurement can and are also to a degree performed on the other modes, they have however been done to a deeper extend for the 26 Hz mode. Especially the calibration, since this is needed for the sensitive gravitational measurements.

4.2.1 Ringdown

Figure 4.3 shows the amplitude data of the 26 Hz mode, showing a spike due to the drive followed up by a drop and a ringdown from a significantly higher amplitude then before the drive. A ringdown was also present before the drive. Three mayor points are marked: The start of the drive (blue), the end of the drive (black) and the start of the ringdown (red). The end is taken as the end of the data set, however this isn't actually where the ringdown ends.

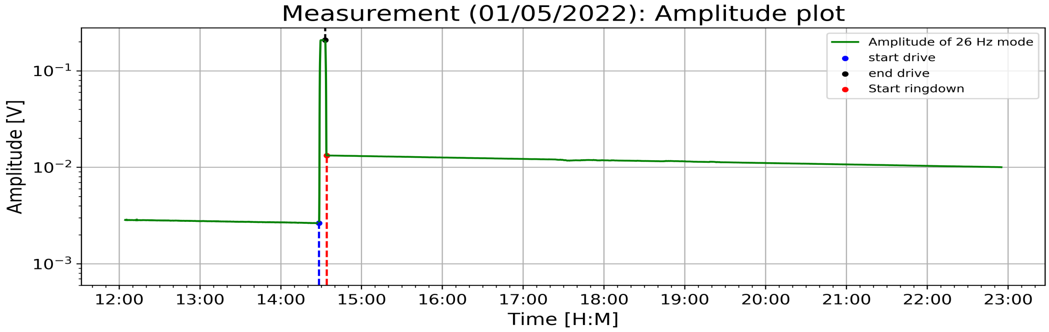

Figure 4.3: *The amplitude data on the 26 Hz mode during a drive and ringdown measurement.*

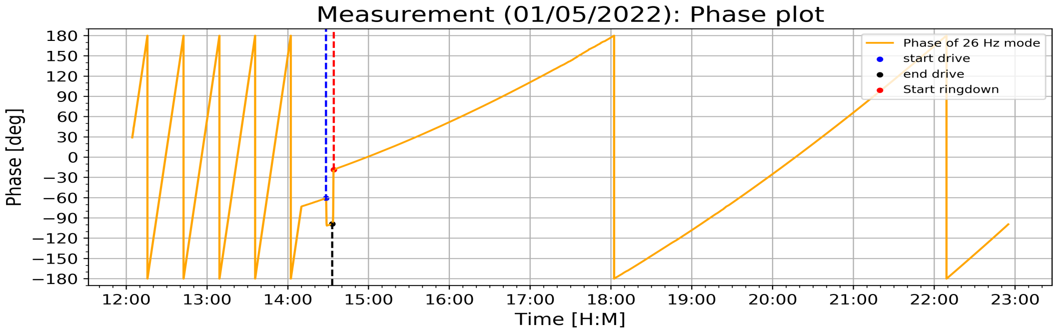

Figure 4.4: *The phase data on the 26 Hz mode during a drive and ringdown measurement.*

Zooming in on the ringdown, between the start and end as set, produces figure 4.5. Over the ringdown a fit is plotted which was achieved with scipy.curve_fit for a function with two parameters (a,b) of the following form:

$$y(t) = a \cdot e^{-t/b} \tag{4.1}$$

Here a is a certain amplitude and b is τ, for this particular plot τ is equal to: 108885 +/- 15 s. Here the standard deviation is the one from the fit. Tau is more then 30 hours, and this is why the end of the ringdown was not visible even in a time trace of several hours.

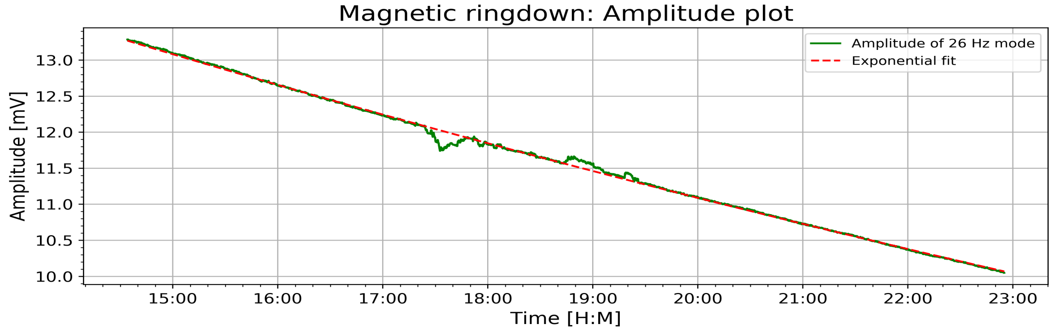

Figure 4.5: *The ringdown following the drive of the 146 Hz mode, showing a clear ringdown which was fitted with an exponential function.*

How good a determination of tau using a fit as above mainly depends on how long was measured compared to how big tau is. To show this a step wise determination of tau has been done to show how the value of the fit progresses for increasing time length. This is shown for 105 steps of roughly 280s in size, these are plotted in figure 4.6.

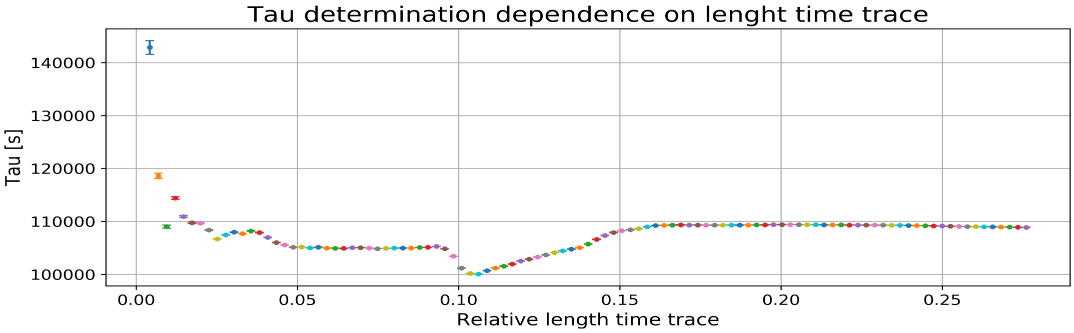

Figure 4.6: *The value of tau given by the fit set out against the relative length of the time trace, a unit less parameter defined as: length time trace/tau. The error on the points is the standard deviation given by the fit.*

This figure clearly shows how the value for tau flattens out for long enough time trace, the effects of the bumps in the amplitude also become visible. This shows that a long and stable enough time trace is important to confidently measuring tau.

Other information which can be extracted from a ringdown measurement lies within the phase data. The data, both amplitude and phase, during a ringdown measurement tends to be more stable. This is due to the higher amplitudes of the movement which dominates over the amplitude of the noise. This allows for a good look at the phase shift, and a phase shift corresponds to a frequency difference between the lock-in and the signal.

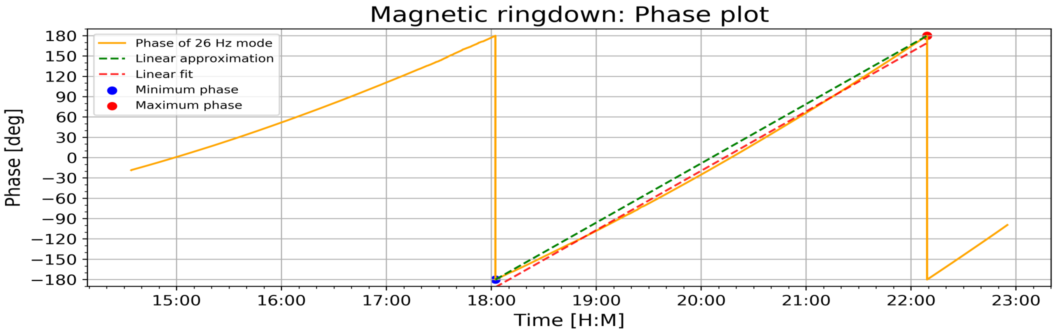

Figure 4.7: *The phase behaviour during the ringdown shows a clear phase shift over time, indicating a frequency difference. Two data points are explicitly marked and between these a fit was performed.*

The phase in figure 4.7 goes through roughly 360 degrees in a time duration of 14810s in between the two marked data points. Now a frequency difference can be determined, using a linear approach for the derivative.

$$\Delta f = \frac{1}{2\pi}\frac{d\phi}{dt} = \frac{1}{360^\circ}\frac{\Delta\phi}{\Delta t} = \frac{359.9^\circ}{360^\circ \cdot 14810s} = 67.52\ \mu\text{Hz}$$

There are two other methods which confirms this results. One is the following line of code: np.average(np.diff(**Data**)) · rate. Where an average is taken of a stepwise derivative which is then correctly scaled with the sample rate. The other is the use of a linear fit ($y(t) = \alpha \cdot t + c$) to this segment of data and look at the value of α. The values returned are 67.52 uHz (np.diff) 67.61 uHz (fit). One of these methods return the same value up to the first decimal, the third (fit) has a different first decimal, 0.1 difference. A safe estimation would be:

$$\Delta f = 67.5 \text{ +/- } 0.1\ \mu\text{Hz}$$

This Δf can be used to adjust the lock-in to a better frequency such that the phase shifts less or even remains roughly steady. This also demonstrates well the scale of precision in the frequency. What must be kept in mind is that these frequencies can shift, this error does not account for that.

Following the determination of τ, the Q-factor can also be determined. The phase shift previously determined can be used to define a value close to the actual resonance frequency, this can be done by adding this shift to the lock-in frequency. Since the lock-in lags behind and therefore the phase increases. The lock-in frequency can be read out from the data set, $f_{lock-in} = 26.6983998$ Hz.

$$f_{res} = f_{lock-in} + \Delta f = 26.6984673 \text{ Hz +/- } 0.1\ \mu\text{Hz}$$

Now the Q-factor can be calculated based on f_{res} and τ. With the correct error propagation this leads to the following Q:

$$Q = \pi f_{res}\tau = 9132812 \text{ +/- } 1229$$

Which is at least a Q-factor of $9.1 \cdot 10^6$, even considering potentially more error. This is a Q-factor of the order of 10^6, almost 10^7, a great result. The Q-factors in other runs were generally of the order of $10^3 - 10^5$, a great improvement.

4.2.2 Coupling

Coupling indicates how much energy can be put into the system, the greater the jump in voltage due to a certain drive the better the coupling. The coupling can thus be derived from a measurement where an effective drive took place.

In figure 4.8, the drive and change in voltage are easy to see. For the strength of the cross talk/drive the average value of the plateau is taken, as indicated by the purple line overlaying the plot of the data.

The quantities that need to be extracted from this data/plot are $\Delta V_{zeppelin}$, V_{drive} and Q_{eff}. A smart insight is that V_{drive} times Q_{eff} is essentially the area of the drive scaled with πf_0, this area is marked in the plot as the orange area.

This doesn't direct match with the plot, however the plot is the signal and this is processed with a low-pass filter which averages. Certain delays are therefore in play, however these happens both at the start and the end of the drive. These are therefore thought to compensate each other enough and in reality the drive is on and off in an instant. As a check an integration was done and as expected these values agreed quite well.

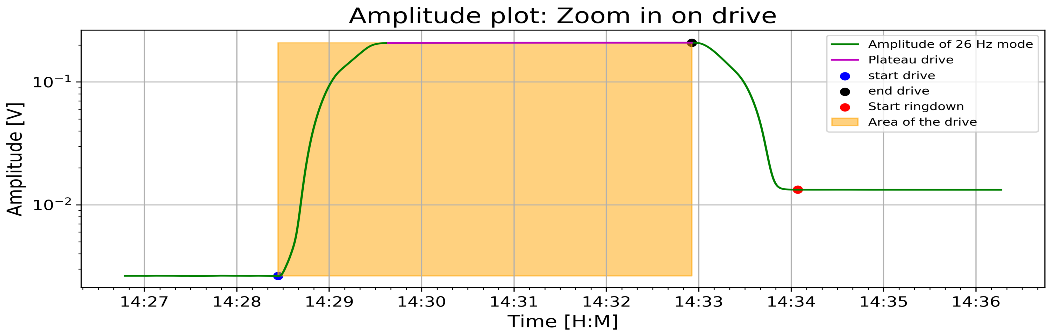

Figure 4.8: *A zoom in of figure 4.3 on the drive, showing how the amplitude of the mode was raised due to the drive.*

What is equally as important is the phase behaviour around the drive. This can be seen in 4.9a, now complex vectors can be made by combining the phase and corresponding amplitudes. z1, z2 and z3 are based on the start drive, start ringdown and plateau of drive respectively. A fourth and a fifth vector (z4,z5) were made by taking the difference of z2 and z3 with z1, these are the drive and displacement vector.

They are visible in figure 4.9b, the during drive/drive vector are for a big part out of the image due to their amplitude being much bigger. The main goal of the figure is to show the approximately 90° angle between z4 and z5, which by theory should be the case. The exact value of the angle between z4 and z5 is: 91.1°, which is indeed close to the theoretical value of 90°.

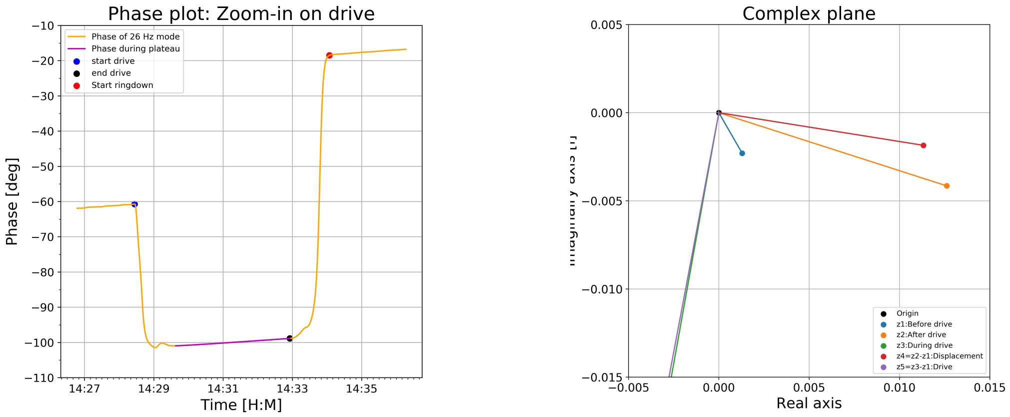

(a) *A zoom in of figure 4.7 on the drive, showing the phase behaviour around the drive.*

(b) *A complex vector plot showing the relevant complex vector and visually displaying the angle between the drive and the displacement.*

Figure 4.9: *Two figures showing the phase behaviour of the drive and how the drive is at roughly a 90° angle.*

From these vectors the coupling can be determined using the following quantities from these vectors.

$$t_{eff} = 268.675131 \text{ s, leading to } Q_{eff} = 22535$$

$$V_{drive} = ||\mathbf{z_5}|| = 206.7 \text{ mV}$$

$$\Delta V_{zeppelin} = ||\mathbf{z_4}|| = 11.5 \text{ mV}$$

This leads to a coupling of:

$$\beta^2 = \frac{\Delta V_{zeppelin}}{V_{drive} Q_{eff}} = 2.46 \cdot 10^{-06}$$

4.2.3 Overview of the modes

An excel was used in which measured values could be put in and the excel would calculate the properties of the different modes based on these inputs. Many of the characteristics of the system where contained in here too. Below a short overview of some of the calculated values are shown, these are calculated in similar fashion as the previous section has shown. However all have not been done to the extend on which the 26 Hz has been measured, analysed and calculated. This due time and focus on the 26 Hz mode, since for this mode the calibration was more important.

Overview of the modes and their most important characteristics				
Frequency [Hz]	**Tau [s]**	**Q-factor**	β^2	**Comment**
15.892	$4 \cdot 10^4$	$2.00 \cdot 10^6$	$2 \cdot 10^{-7}$	-
26.698	$1.08 \cdot 10^5$	$9.13 \cdot 10^6$	$2.46 \cdot 10^{-6}$	suspected z-mode
40.622	$1.39 \cdot 10^4$	$1.77 \cdot 10^6$	$7.84 \cdot 10^{-6}$	-
55.148	$3.27 \cdot 10^4$	$5.66 \cdot 10^6$	$1.28 \cdot 10^{-6}$	-
129.096	$2.2 \cdot 10^3$	$8.72 \cdot 10^5$	$1.23 \cdot 10^{-8}$	suspected rotational
146.590	$1.5 \cdot 10^3$	$6.91 \cdot 10^5$	$4.72 \cdot 10^{-8}$	suspected rotational

4.2.4 Calibration

A table showing the calibration quantities from the excel sheet used to calculate the sensitivity, which is at the bottom of the table.

Calibration quantities and their origin		
Variable	**Value**	**Origin**
β^2	$2.46 \cdot 10^{-6}$	experimentally determined
L_{tot}	$7.91 \cdot 10^{-7}$ [H]	Sum of the inductances in the circuit
k_z	$7.91 \cdot 10^{-7}$ $[\frac{N}{m}]$	mode property ($k_z = mw_z^2$)
V/Φ_0	0.43 $[\frac{V}{\Phi_0}]$	SQUID property
I/Φ_0	$5.00 \cdot 10^{-7}$ $[\frac{A}{\Phi_0}]$	SQUID property
I/z	$1.95 \cdot 10^{-1} [\frac{A}{m}]$	$\sqrt{\beta^2}\sqrt{\frac{k_z}{L_{tot}}}$
Φ_0/z	$3.90 \cdot 10^5$ $[\frac{\Phi_0}{m}]$	(I/z)$(I/\Phi_0)^{-1}$
V/z	$1.68 \cdot 10^5$ $[\frac{V}{m}]$	$(V/\Phi_0)(\Phi_0/z)$
z/V	$5.97 \cdot 10^{-6}$ $[\frac{m}{V}]$	$(V/z)^{-1}$

4.3 Gravity measurements

This section will step by step go through the analysis of one of the gravitational measurements, clearly showing the steps taken during the data analysis and shortly mention why based on previously explained theory.

4.3.1 Analysis of a measurement

The analysis will be done on what is known as the measurement on pos4/H1, this means lateral position four and vertical height one. This format is also handled for the other measurements and the numbering is chronological. This measurement was chosen because all the important and taken steps during the data analysis are well shown and where clearly needed to lead up to the improved result.

Raw data

The start of the analysis begins with looking at the raw data. In figures 4.10 and 4.11 the raw data is plotted. A dip in the amplitude of the laser is visible, which also shows in the phase data as more turbulent phase behaviour. This was due to the mass wheel losing its lock on the frequency for a short while. This happened relatively early in the time trace and was therefore easily cut out. The phase data also shows the difference in the frequency of the zeppelin, laser and the lock-in. Since the phase data of the zeppelin is nearly flat due to the lock-in frequency being extremely close to the frequency of this mode. The laser however experiences a significantly higher phase shift, which is visible in how quickly in cycles through 360 degrees a lot of times during the time trace. This is because as mentioned

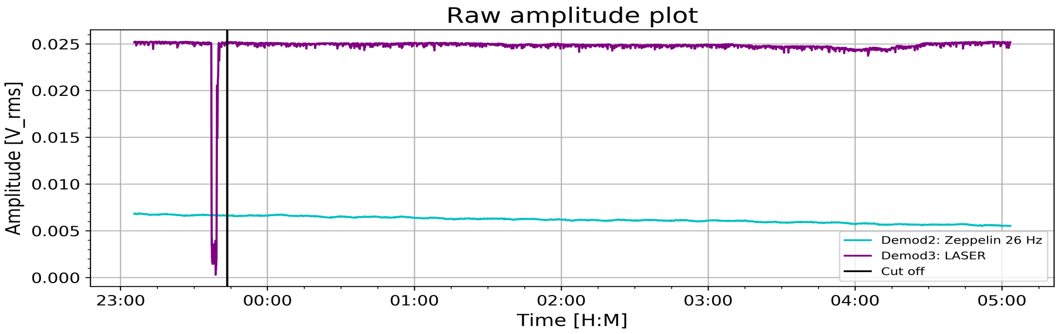

Figure 4.10: *The raw amplitude data of 26 Hz mode belonging to the zeppelin and the data on the laser. The black line showing, is where the data was cut off.*

before the wheel is set a frequency slightly off set to the frequency of the zeppelin.

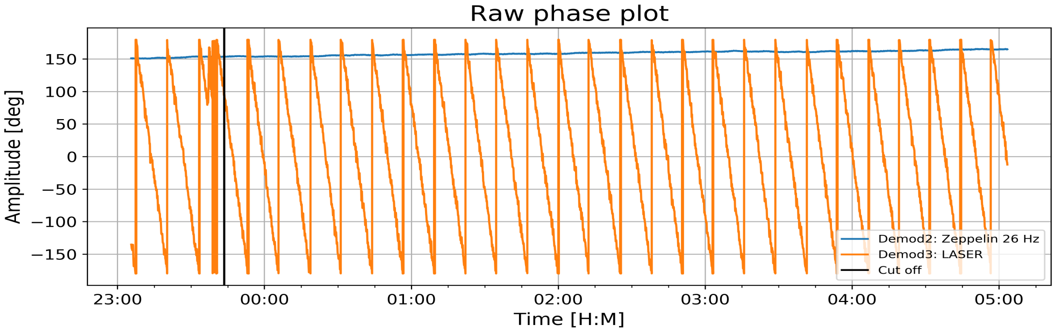

Figure 4.11: *The raw phase data of the mode and laser. Showing the phase shift of the demods.*

From this raw data, complex numbers can be made from which a FFT can be taken. In the FFT any potential gravity signal should be visible on a slight off set to the peak of the zeppelin, coinciding with the center peak of the laser. This FFT is shown figure 4.12, now it also becomes apparent why the wheel is set up with a slight off set.

A small peak rises above the noise level coinciding with the maximum of the FFT of the laser. What is however also visible in this plot is the spectral leakage, this is mainly apparent in the FFT of the laser. By looking at the phase data is becomes clear why this is, the phase is non periodic for both the zeppelin and the laser. For the laser however the spectral leakage is greater because the difference in phase is greater.

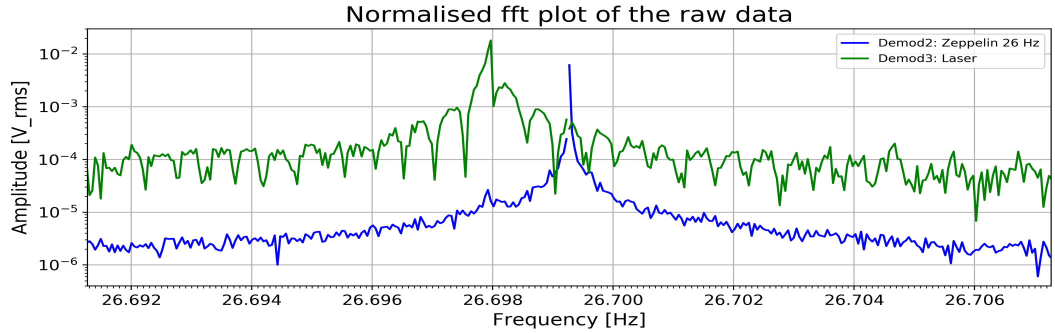

Figure 4.12: *A normalised Fast Fourier Transform spectrum shown around the frequency of the lock-in +/- 0.01 Hz, the normalisation happens through dividing by the length of the data-set. Spectral leakage is especially visible in the plot of the laser.*

Ringdown correction

There are several steps which need to be taken to improve data. Two of the methods viable of for this where already shown in the section about the ringdown. The laser amplitude ofcourse doesn't undergo a ringdown, however the zeppelin does. This ringdown is clearly visible in the raw data, it becomes more apparent when only the amplitude of the zeppelin is plotted with different y-axis. This plot and the fit which was done on this data can be seen in figure 4.13.

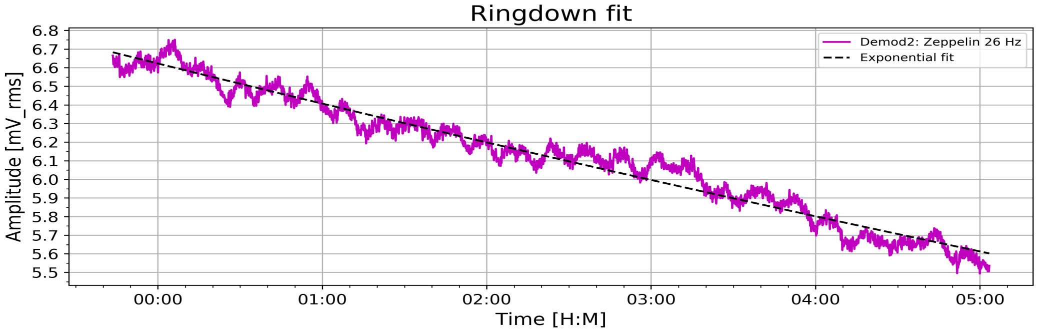

Figure 4.13: *The amplitude data of the zeppelin after cut off. On this data an exponential fit was performed which is plotted over the data.*

This ringdown can be subtracted from the data using the following algorithm:
New amplitude = Old amplitude - ringdown fit + amplitude parameter

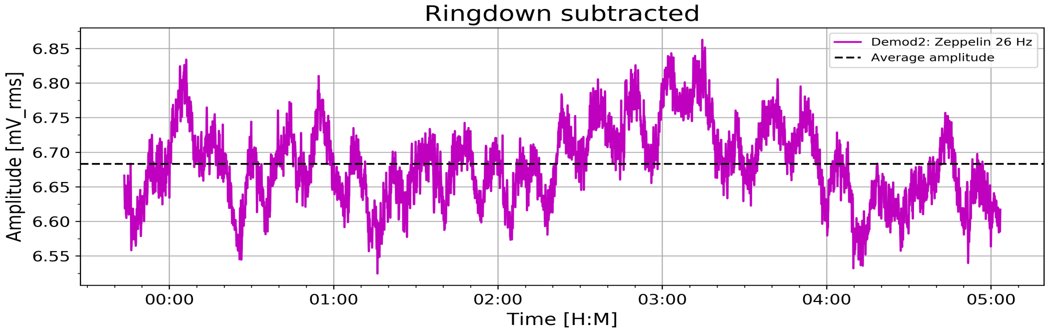

Figure 4.14: *The resulting amplitude data after the ringdown has been subtracted, the average has been plotted as well to show how the data oscillates around this constant value.*

This algorithm creates a new data set in which the data oscillates around a certain constant value, without the steady decrease due to the ringdown.

The results of this algorithm can be seen in figure 4.14.

This constant value doesn't influence the gravity signal since this is hidden inside the oscillations and the amplitude of these oscillations don't change. This value is added since else the FFT of the zeppelin would miss its center value for frequency of the mode.

The reason to correct for this is again spectral leakage, both the phase and the amplitude play a role in this. Since the FFT is done based on the complex numbers which are formed from the phase and the amplitude.

Phase&frequency correction

In the section on the ringdown two other corrections were made, the phase shift was corrected and the frequency was adjusted accordingly. It is important to mention that the shift for which the phase of zeppelin has been corrected was also subtracted from the phase of laser, since the difference between these two must hold.

Before the correction is done on the phase of the zeppelin, an intersection point between the two phases on each end of time trace is picked. Choosing this intersection makes sure that the phase of the laser is also corrected, although slightly less since these intersections are not precisely on top of each other. This results in figure 4.16. Please note that the variations in both the amplitude and phase with a period of approximately five oscillations per hour are due to the rotation of the wheel.

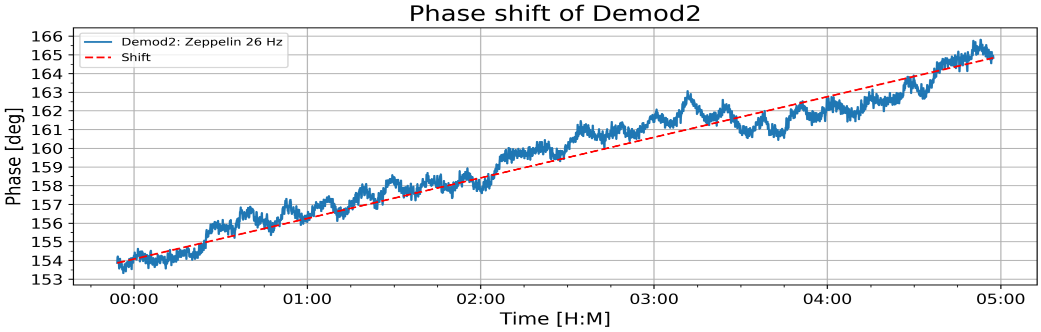

Figure 4.15: *The phase of the zeppelin over which a linear shift has been plotted which ties the two ends together.*

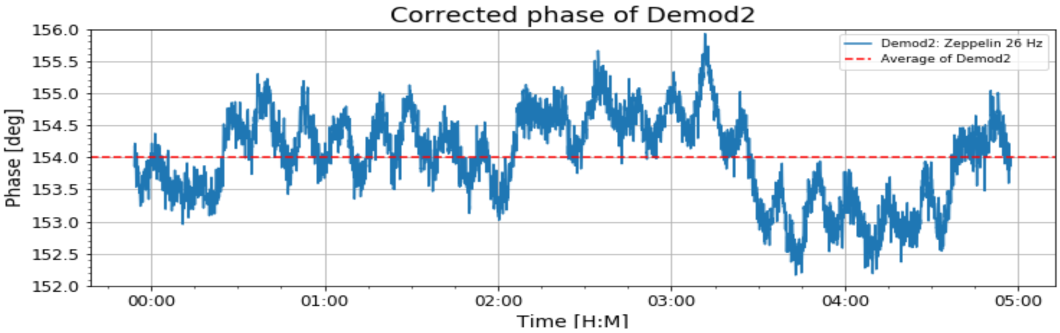

Figure 4.16: *The phase of the zeppelin after correction, visible more flat. There are small oscillations visible in the phase.*

Improved FFT

These steps should decrease the spectral leakage and improve significantly on figure 4.12, the resulting FFT is indeed much better and can be seen in figure 4.17. The sharpness of the peak of the laser has increased tremendously, and the signal to noise ratio of the small peak in the FFT of the zeppelin seems to have improved slightly as well. While in figure 4.12 it is roughly a factor of 3 above the surrounding noise, it is now a factor of 10 above the surrounding noise

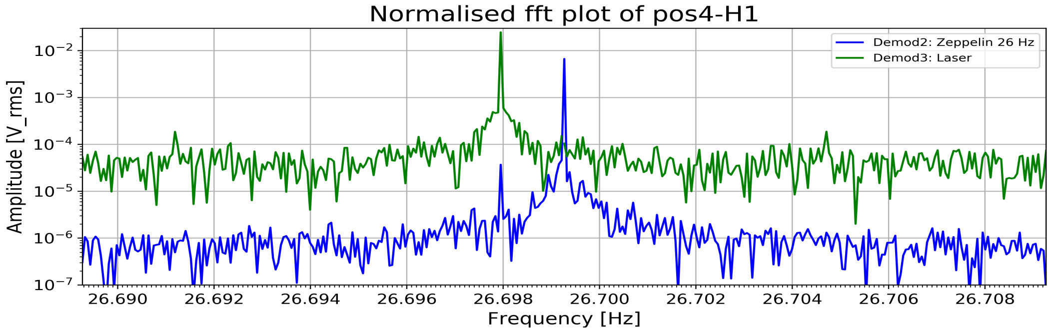

Figure 4.17: *Figure of the improved FFT after steps had been taken to decrease spectral leakage. The improvement is significant when comparing the two figures.*

The local maxima of the zeppelin and the global maxima of the laser perfectly coincide at a frequency of f_{signal} = 26.697952 Hz. Furthermore the global maxima of the zeppelin is the resonance frequency, the signal is offset to this with $\Delta f_{offset} = f_{signal} - f_{res}$. These values including the frequency resolution are included in the table below. For the other results in the appendix, they will be included in the caption.

Important FFT quantaties		
Variable	**Frequency value [Hz]**	**Origin**
f_{res}	26.699271	Resonance frequency of the mode.
f_{signal}	26.697952	Coinciding frequency signal and laser
Δf_{offset}	-0.0013	The offset of the signal
df	$5.5 \cdot 10^{-5}$	Frequency resolution

Note f_{res} slightly differs to calibration measurement.

Unit conversion

The next step is to convert the voltage read out to the proper units, namely Newtons. This is only relevant for the FFT of the zeppelin, since the laser is solely an electrical signal on which no actual conversion is needed or relevant. This conversion happens based on previously determined quantities of the mode, through the calibration. Furthermore the gain needs to be accounted for, this was set at 10 and needs to be divided out again. To convert the V_{rms} to m_{rms} a simple scaling with the sensitivity and 1/gain is done.

This scaled down FFT and the transfer function have been plotted in figure 4.18, they are graphically represented in such a way that the transfer function overlaps to great extend with the FFT. This shows the correlation between these two and furthermore shows how the signal pop out above the transfer function. For precisely this reason the slight off set was chosen, since this makes it easier to distinguish a signal from the Lorentzian then when it adds to the peak of the mode.

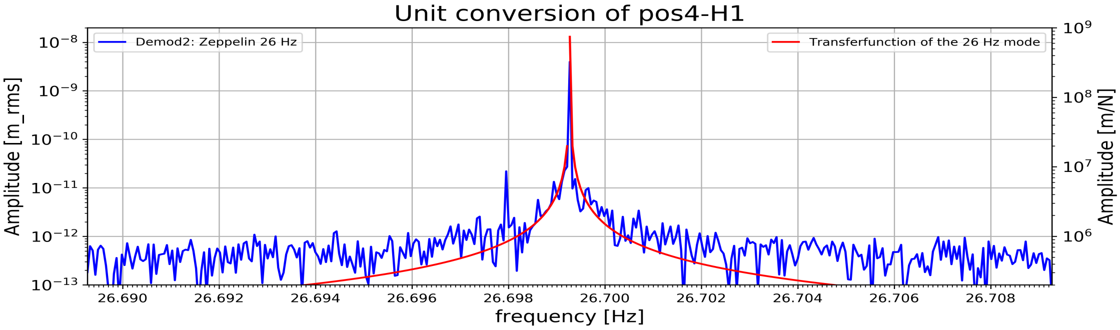

Figure 4.18: *Scaled FFT of the zeppelin with the overlaying transfer function. Showing a clear correlation between the center peak of the mode of the FFT and the transfer function.*

What is important to mention here is that the transfer function was plotted for several different Q-factors, for high enough Q-factor the transfer function didn't change significantly anymore when increasing the Q-factor even more. This is especially true for the transfer function at the frequency where the signal generally is measured. I.e. changing the Q factor from the current 9 million to 5 million or to 50 million only changes the shape of the transfer function in the close vicinity of the peak value. WHich is not within the resolution of the spectrum anyway. This means that the Q factor is not important for the transfer function at the frequency of the signal.

The final step is to divide the FFT by the transfer function, this leads to an FFT in N_{rms}. Which can be seen in figure 4.19, this shows the signal as a distinct peak above a noise floor. The amplitude and phase of this peak are important, these are saved and will be compared to the other data points on the different positions. The other final plots on the other positions are visible in appendix B.

At this point two errors are introduced, error1 and error10. These are based on the average value of 1 point on each side of the peak or on 10 on each side. The error1 is more insight full when it comes to leakage effecting the signal, whilst the error10 captures the noise level better.

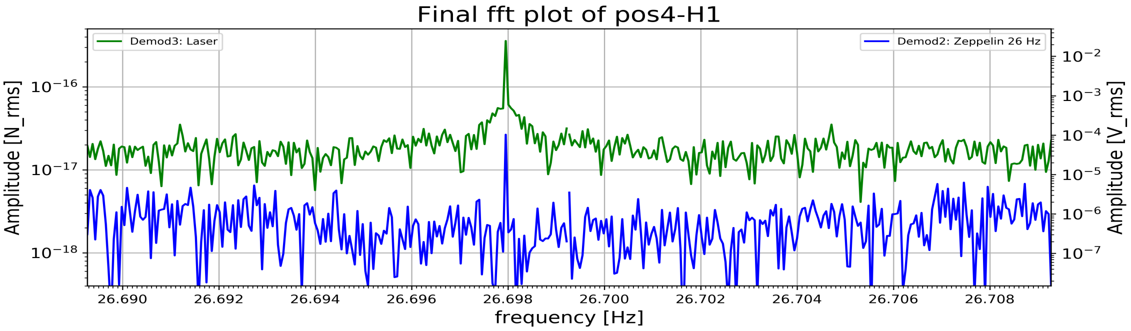

Figure 4.19: *The final FFT plot showing a signal in Newtons above the noise floor.*

Noise

A noise spectrum can be made through dividing by $\sqrt{df}$, this is only done for the zeppelin. This produces the figure below.

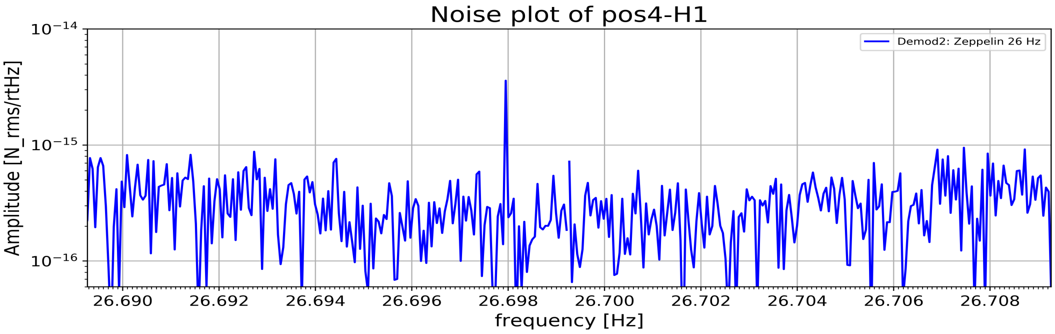

Figure 4.20: *Noise spectrum: showing how the noise floor is of approximately 0.2-0.4 fN.*

Similar noise levels were seen for most of the other plots, with an upward trend for higher measured amplitudes. Ranging from 0.2fN to 1fN noise.

4.3.2 Analysis on different heights

Now a separate analysis can be done on the vertical displacement of the wheel. These are the data points on lateral position 5 (pos5) with different heights (H1-H5), of which the approximate values are shown in the table below.

Vertical data point on pos5			
Position	**Amplitude [aN]**	**Phase [°]**	**Vertical distance [cm]**
H2 (N-5)	9.49	3.7	57.1
H3 (N-3)	13.25	5.7	53.5
H4 (N-1)	26.43	26.4	49.9
H1 (N)	28.54	-3.1	48.1
H5 (N+1)	28.60	10.9	46.3

This group of data point is plotted in figure 4.21 and 4.22, the first being the amplitude plot and the second the phase plot.

In the first figure two curves are plotted as well. These curves are the simulated curves for the expected RMS force, one is the original and the other is a scaled down version. Is clear that the data points fall short to the original curve, the scaled down version shows by approximately how much. This scaled down version is the original one divided by a factor of 2.5. What is promising though is how the data point are arranged, they seem to roughly abide to the expected behaviour.

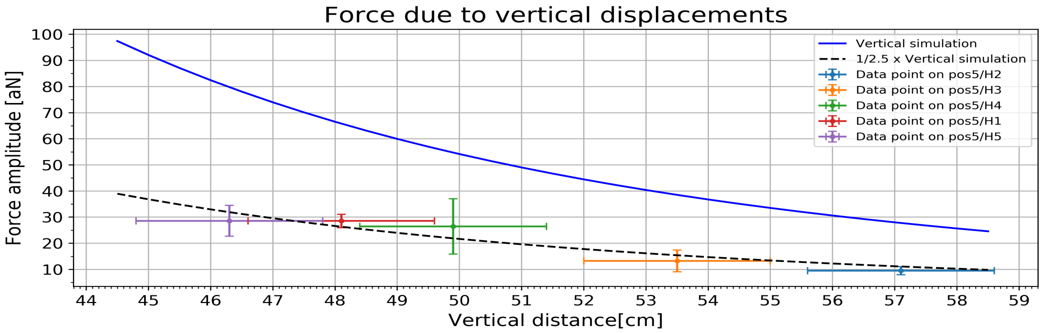

Figure 4.21: *The measured force set out against the estimated vertical distances for the different heights on pos5.*

The y-error used the error10 introduced in the previous subsection. The x-error is the error in the estimation of the vertical height, not an error in the difference between the heights.

This error is based on how the estimations were made and the fact that the exact shrinkage of the springs inside the cryostat is unknown. The error is estimated at 1 to 2 cm and is set at 1.5cm in this plot. The difference between the heights is due to the planks and these are known with mm precision, more accurate and thus a less significant error.

In the phase plot the vertical simulation is plotted together with the data points. The errors in the phase are based on the errors in the amplitude, according to: $\frac{180}{\pi}\frac{error}{amplitude}$.

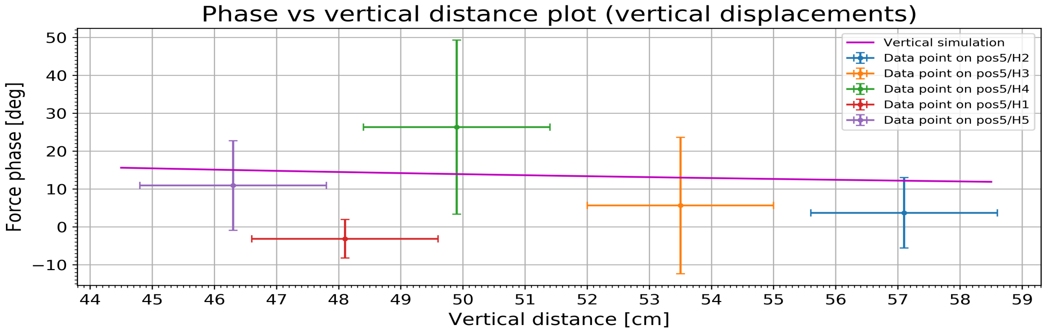

Figure 4.22: *Phase of the five heights set out against the vertical position, the curve shown is the phase simulation for vertical displacement.*

4.3.3 Analysis on different lateral positions

A similar analysis can be done for the data points on height H1 for the different lateral positions (pos2-pos5), this set can be seen below. This set of data points is also plotted in figure 4.23, together with two curves.

Lateral data point on H1			
Position	**Amplitude [aN]**	**Phase [°]**	**Lateral distance [cm]**
pos2	21.25	-48.4	-11
pos3	16.06	137.8	14
pos4	26.61	42.6	3.5
pos5	28.54	-3.1	-3

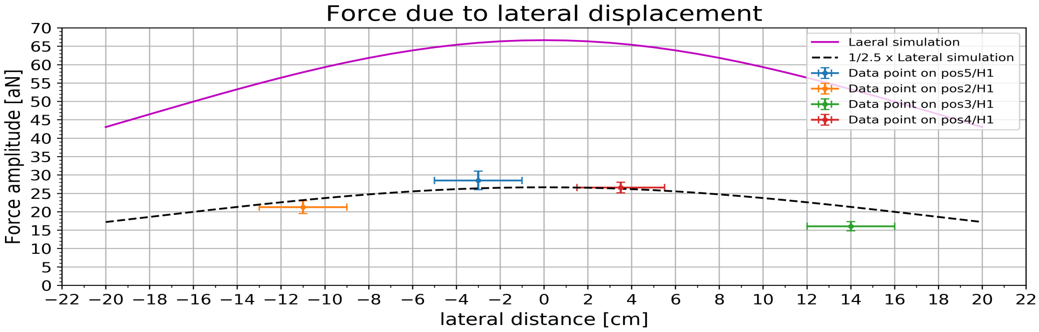

Figure 4.23: *Amplitude plot combining the simulation with the four data points on posX/H1. Showing how the points seems to roughly drop off in the correct fashion with increased lateral displacement.*

The points again fall short of the simulation, however their arrangement looks to correspond to the curve. Similar to before a down scaled version of the simulation is plotted as a dotted line. The down scaling is again done with a factor of 2.5, the same as with the vertical analysis.

The x-error for the lateral displacement is set at 2cm and is independent per point since these positions are estimated separately. The y-error is the achieved the same way using the error10 as before.

For the lateral displacement the phase behaviour is of more interest then for the previous vertical displacement. This is plotted in figure 4.24, in this figure two lines are included. The lateral simulation and a guess line, the latter is a line which was plotted and seemed to better align with the data points. This is not a fit though, it is to visualize the difference between the data points and the simulation. This line also doesn't go through the origin like the simulation, which in theory should be the case.

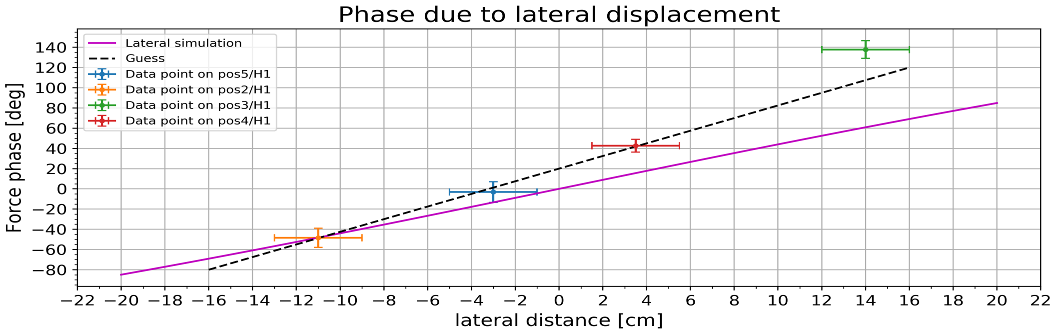

Figure 4.24: *Phase plot for the four data points on posX/H1, plotted together with the simulated line and a guess.*

Chapter 5

Discussion

In this chapter the major results will be discussed and point of discussion are addressed. The major points that are addressed are:
1) Q-factor
2) Coupling
3) Gravitational measurements

5.1 Q-factor

From the ringdown measurement tau, f_{res} are derived to determine the Q-factor. How well were these determined and did this lead up to an accurate determination of the Q-factor.

Tau was already estimated at roughly 10^5 s using simple estimations based on the live data. The fit was done on a time trace of 30058 s, which returned $\tau = 108885$ +/- 15s. The big factor in determining a tau is the time measured compared to how big the tau is, this was shown in figure 4.6.

Seeing how stable the measurement was and that the value of tau seemed to converge to a roughly constant value, is safe to say that tau has been determined with good enough accuracy. The debatable value is the standard deviation given by the fit, since 15 seconds on a tau of 100ks is extremely accurate. This is however not so significant since even a 10 or 100 times bigger error is sufficient enough on a tau of 100ks.

The resonance frequency is approached using a ZI lock-in amplifier, which operates with great precision. This was done in addition with an 10 MHz atom clock, which is even more precise. Any significant error therefore is most likely a human error. The resonance frequency is determined by addition of a frequency shift based on the phase to the lock-in frequency. The lock-in frequency is highly accurate and outside of our influence. The determination of the shift isn't, this shift was however determined in three ways to prevent any accidental error made on just one determination. These three methods agreed well, two even agreed up to 0.01 μHz. Importantly, the resonance frequency does shift when warming up to more then 10K and cooling down immediately. In that case the resonance can shift by several Hz, which we attribute to flux getting trapped in the superconductor. This is due to inhomogeneities of the critical temperature in combination with a temperature gradient during the cooling down of the trap.

In comparison with the determination of tau, the resonance frequency is not the major factor in the determination of the Q-factor. This was checked using the proper error propagation, not propagating the error in the resonance frequency and just linearly propagate the error in tau hardly made any difference (0.12s difference). This actually also holds for the frequency shift in general, taking the lock-in frequency is actually already more then good enough.

The safe estimation made was at least a Q-factor of $9.1 \cdot 10^6$, this Q-factor is more then high enough that even an error of 1Ms would not significantly influence the transfer function, especially at the frequency of the signal. The error in tau even if it is 100 bigger, would only then produce an error of 10^5 on the Q-factor. At which point it start to become a significant error on a Q-factor of $9.1 \cdot 10^6$, it still remains insignificant for a Q this high with regards to the transfer function.

5.2 Coupling

Another important quantity is the coupling, which was determined from a magnetic drive. The value derived is $2.46 \cdot 10^{-06}$, which is one of the highest couplings achieved for this experiment. An important mention here is that $Q\beta^2$ is greater than one, which is relevant when it comes to the detection noise of the SQUID. In general this can pose an issue, however no severe effects were noticed.

The value was derived using complex vectors based on the phase of the signal at certain time points. The choosing of these points is subject to potential human errror, the points that were chosen were also made with the support of the derivative of the data. The derivatives for both the phase and amplitude give a good indications whether the point is at the correct place. Since the turning on and off of the drive is a huge change.

On top of this the phase was chosen as the leading argument, since the rate of change was higher for the phase outside the drive making it's influence greater.

On top of this several checks can confirm that the points were chosen in a good enough manner. One is direct shown in the results section, which is the resulting angle of 91.1°. This value is very close to the theoretical 90° and confirms that the value of the points are indeed very close to what they in theory should be.

One of the other choices that was made is the interval on which a average was taken. This was done because the phase and the amplitude were not as flat as they could and should be. This was due to the fact that a ring-down was prior to this measurement in effect. This is especially visible in the phase data, for this could be corrected however taking an average was deemed viable enough.

Another check that was made is the on the value of $V_{drive}Q_{eff}$. The claim was made that the area in orange was the actual drive and should correspond to the area under the amplitude curve, which was shaped differently due to delay effects. The check value was determined as via $V_{drive}Q_{eff}sum = \frac{R_{sum}\pi f_0}{rate}$. Which is effectively taking an integral an scale it with πf_0. The value used was 4658 V and the check returned a value of 4552 V, a small difference of just 2%.

This doesn't mean the value for the coupling is the actual value. The determination of the value is done in a correct manner, based on the measured values. Behind these measured values are however many variables at play. A current hypothesis is that potentially some field might be leaking from the calibration transformer. This would couple in more field into the confinement, onto the zeppelin and pick-up coil. This could mean that the coupling is determined as too high. The sensitivity of the experiment goes as $\frac{1}{\beta}$, a lower coupling means higher sensitivity. Higher sensitivity means that actually more motion was present and the measured gravitational amplitudes should be higher.

5.3 Gravitational measurement

The biggest errors and uncertainties lie within the gravitational measurement. There are two major points when it comes to the gravitational measurement, these are the data analysis of the gravity data and the simulations. On the base of a simple comparison of what is seen compared to what is expected.

Spectral leakage

When it comes to the data analysis two factors, the Q-factor and the coupling, have already been discussed and are measured well enough. These play a role in the unit conversion, a huge part of the data analysis was the prevention and systematic removal of spectral leakage. This was done with two correction, one to the amplitude and one to the phase.

The phase correction is a simple correction which results in the start and end value simple being tied together. Which is precisely what is needed for the reduction of spectral leakage. How true this is to the actual shift is debatable. What is however also debatable is how constant this shift remains during a time trace of several hours. In the example analysis there seems to be a sudden change at around 03:20, after which is seems to roughly propagate in similar way as before. Changes such as this are hard to prevent and also not easily corrected. However in the end it is all about the small oscillations in the phase and these are as good as uneffected.

The correction to the amplitude was the subtracting of the ringdown, this was done with a fit. This is different to how the phase was corrected and does not directly tie the start and end point to each other. However the oscillations are quite small which makes any potential step not big, thus not creating much spectral leakage. What is an advantage of the fit is that the amplitude can be set as a fit parameter. This allows to add this back to the data after subtracting the ringdown. Although the oscillations still remain, not adding this value back up would create an FFT with out the huge peak value at the resonance frequency. Which would create a huge dip after dividing with the transfer function. In the end the result speaks for it self, in general the improvement from the raw FFT to the FFT after the corrections were made are more then significant.

Vertical and lateral displacement

The speartip of the result section and the data analysis is the analysis on the different positions, vertical and lateral. Here the expectations are directly compared to what is measured.

For both the vertical and lateral displacement of the mass wheel there was roughly a factor of 2.5 difference between the data points and the simulation. This would suggest a systematic mistake in either the simulation of the calculations of the amplitude of the data points. What is worth a mention is that the data analysis was first done using a derivative and scaling according to a derived formula. This was done on pos2/H1 where for the first time a signal was seen, compared to the results via the transfer function this does not explain a factor of 2.5. It might be interesting to compare these methods.

Nevertheless apart from their absolute value, the data points behave in the expected manner. For vertical displacement the value drops off with increasing distance and for the later displacement the amplitudes drop off with increasing distance from the center.

For both the error in the displacement is quite significant, this is certainly worth improvement as it becomes a necessity now. For the vertical this might be tougher since this has to do with the cryostat being closed and cold thus shrinkage of the springs. An extra factor that needs to be accounted for is any possible lateral displacements during the changing of the height. What does help here is the fact that the vertical displacement is of bigger impact then lateral displacement. Next to this most steps in the vertical displacements were 3.6cm (2 planks), this would dominate any small lateral displacement. Any lateral displacement is within the order of the error. The influence of the lateral displacement is however of bigger influence on the phase.

Now on to the phase behaviour of both the displacements. For the vertical displacement the data points are indeed relatively closely arranged and are not far off with respect to the simulation, the errors are however very big. In comparison to the lateral displacement, where big phase changes are expected, the phase changes are comparatively small.

The effects of any lateral displacement are however of bigger impact on the phase then on the amplitude. The data point which shows this the best is pos5/H1, after this data point was acquired 5 planks were removed. This was the biggest vertical step taken, and very likely to have suffered the most lateral displacement. This data points falls quite short in comparison to the other data points.

For the lateral displacement the phase changes are indeed bigger, however also steeper then the simulation. This is shown by the difference between the guess and simulation line. The guess line does not go through zero, however the laser is thought to be offset by 5 to 8 degrees. Which brings us to another point of discussion, how good is this laser and the feedback on the wheel. From the FFT's on the laser the peak is mostly quite sharp. It does however have significant shoulders, in most measurements. A certain width of signal directly around the peak, which still sits well above the noise. The stability with which the mass wheel influences the same frequency ofcourse matters for the measured result. Especially when even higher frequency resolution is achieved.

An other big factor that could play a role in phase behaviour is the alignment of the mass wheel and the confinement. Since the influence of the mass wheel on the phase differs for displacement in x or y. Rotating the mass wheel on a fixed lateral position might be an interesting test. The behaviour of a lateral mode can be quite similar to that of the vertical mode, as was shown by Dennis his work. It remains hard to make this distinctions since the data points are not spot on with the expectations.

A point worth addressing is the fact that the rotational modes are not well known. There is a certain insight on how the frequencies would roughly behave, based on this argument the glass ball was added to the zeppelin in the manner that it is. What is not known is the influence of the mass wheel on these modes.

Chapter 6

Conclusion

Our main objective was to develop a micromechanical resonator which would be able to detect the effects of gravity on extremely small scale. This would best be achieved through measuring the vertical mode while influencing it with a mass wheel. To achieve this first several developments have been made with the aim of increasing the Q-factor of the system.

These major developments were made on the zeppelin and the vibration isolation during several runs and proved fruitful. Since these eventually led to run28. This run produced a great spectrum in which the vibrational modes were easily visible and found through magnetic drive in quick succession. After which several characteristics of several modes were determined. This allowed to make a consideration on which mode would be used for the gravitational measurements. This consequently led to a closer look at the 26 Hz mode.

For the 26 Hz mode the following important quantities where determined. A Q-factor of $9.13 \cdot 10^6$ is measured as a consequence of a tau of $1.08 \cdot 10^5$ at a frequency of 26.698 Hz. Which is several orders higher then previous runs, an excellent improvement. From the same measurement the coupling, β^2, is determined at a value of $2.46 \cdot 10^{-6}$.

With these promising signs, the mass wheel was set up to influence this mode of the zeppelin. This led to a first signal being visible in the FFT spectrum of the data. After which several different measurements on different position were done. From these measurement amplitude are measured in the range of 10 to 30 attoNewtons. Together with the phase behaviour a comparison is made with the expectations. This comparison is however not fully conclusive, since the data points fall short of the simulation. Furthermore the alignment of the trap and the mass wheel plays a big role in the behaviour of the lateral modes for any displacement, this does not rule out the lateral modes.

Unfortunately which mode has been measured can not be said at this stage. Further simulations and measurements could give insight on this. The alignment of the mass wheel and the trap need to be taken into account. The current data can be compared to such new simulations. Further measurements can be done where the mass wheel is rotated at a fixed lateral position underneath the cryostat. This could provide a possible measure to distinguish the translational modes better. Since this proved not possible at the time.

Nevertheless repeatedly a signal has been measured. Which can be said to behave as a translation mode under the influence of a mass wheel. No big discrepancies exist between the amplitude and phase behaviour, as was a problem before. This holds both for the vertical and lateral displacements. Considering all these factor and how the data presents itself, it can be said that an actual gravitational interaction has been measured between a mass of 0.433mg and 2.4kg. Which means a huge step has been made with regards to the development of this system, which is now capable of measuring extremely small gravitational interactions.

Acknowledgement

Ik wil graag iedereen bedanken die heeft bij gedragen aan dit mooie project. Ik samen met Tjerk kunnen voortbouwen op het werk wat mede door Jean-Peal en Dennis is gedaan in de afgelopen jaren. Het een op een persoonlijk samenwerken met Tjerk is een privilege die niet voor veel bsc studenten is weg gelegd. Naast dat dit ook ontzettend leuk is, was dit ook uiterst leerzaam. Verder wil ik Tjerk ook graag bedanken voor zijn vertrouwen in mij, jij liet mij al gauw knutselen aan van alles. Als dat gene waar je dan aan mag knutselen een met goud bekleden cryostaat is dan is dat stiekem toch heel erg cool. Het met mijn handen werken vond ik zelf ook erg leuk, de engineer in mij kwam naar boven. Toch was bij iedere stap eerst nagedacht over het theoretische effect ervan. Deze combi van knutselen en theoretisch brainstormen is iets wat ik erg leuk heb gevonden aan deze bsc stage.

Verder wil ik de groep ook graag bedanken voor hun gastvrijheid en behulpzaamheid. Ik keek ook menig keer met nieuwsgierigheid naar wat er om mij heen gebeurde. Zo ben ik wel een paar keer bij Koen aangeschoven, heeft Tim mij ook van alles laten zien en keek ik ook een keer mee bij een leuek meting van Jaimy. Verder wil ik natuurlijk Louw en Alexander ook niet vergeten, voor de gezamelijk uurtjes in de nieuwe meethal, de wandeltochten met of zonder vat helium dan wel niet stikstof of de gezamelijke lunches. Ik hoop dat zij hun bsc stage net zo leuk ervaren hebben als ik, daar heb ik wel het vertrouwen in net als de mooie resultaten die geboekt zijn.

Al met al een heel leerzaam en leuk half jaar, iets wat mij laat uitkijken naar mijn master stages. We zullen elkaar vast nog wel eens zien en spreken. Verder ben ook zeer benieuwd naar de ontwikkelingen die nog gaan komen aan dit project, waar ik toch een beetje mijn ziel aan verkocht heb.

Ik heb genoten, de groeten
Noud van Halteren

Bibliography

[1] B. van Waarde, *The lead zeppelin : a force sensor without a handle,* Technical report, 2016.

[2] A. Vinante, P. Falferi, G. Gasbarri, A. Setter, C. Timberlake, and H. Ulbricht, *Ultralow Mechanical Damping with Meissner-Levitated Ferromagnetic Microparticles,* Physical Review Applied **13** (2020).

[3] *Superconductor interactions with magnetic field*, 2011.

[4] K. Takasugi, H. Sakai, M. Ooshima, D. Noda, and N. Asakawa, *Development of contactless dynamic spindle testing using an eddy current brake,* Precision Engineering **74** (2022).

[5] A. A. Kordyuk, *Method of images*, 2004.

[6] D. Griffiths, *Introduction to Electrodynamics,* Cambridge University Press, Cambridge, Verenigd Koninkrijk, 2017.

[7] J. van Soest, *Meissner Levitated Magnetic Microparticle,* Technical report, 2020.

[8] B. Jervis and E. Ifeachor, *Digital Signal Processing :: A Practical Approach 2ND EDITION,* Prentice Hsl, Inc.,2002, 2002.

[9] *NC-1 - Magnicon Research and Instrumentation - SQUID electronics, SQUID sensors, SQUID systems*, 2007.

[10] D. Uitenbroek, *Meissner Levitating Micro Particle,* Technical report, 2021.

[11] Supermagnetman, *C0005-10 micromagnets*, 2020.

[12] SM Magnetics, *Sintered NdFeB - Neodymium Iron Boron*, 2020.

Appendix A

Derivations

A.1 London penetration depth

Here the London penetration depth will be derived from the second London constitutive equation, equation A.1, and using two of the Maxwell's equations. The two Maxwell equations are Ampère's law, equation A.2, and the no-monopole law, equation A.3.

$$\nabla \times \mathbf{J} = -\frac{n_e e^2}{m}\mathbf{B} \tag{A.1}$$

$$\nabla \times \mathbf{B} = \mu_0 \mathbf{J} \tag{A.2}$$

$$\nabla \cdot \mathbf{B} = 0 \tag{A.3}$$

The first two equation can be combined by taking the curl of equation A.2.

$$\nabla \times (\nabla \times \mathbf{B}) = \mu_0 \nabla \times \mathbf{J} \tag{A.4}$$

Using the following vector calculus identity for any **V**:

$$\nabla \times (\nabla \times \mathbf{V}) = \nabla(\nabla \cdot \mathbf{V}) - \nabla^2 \mathbf{V} \tag{A.5}$$

this leads to an equation where we can apply the no-monopole law, equation A.3, on the left side and the second London equation, equation A.1, to the right side.

$$\nabla(\nabla \cdot \mathbf{B}) - \nabla^2 \mathbf{B} = \mu_0 \nabla \times \mathbf{J} \tag{A.6}$$

$$-\nabla^2 \mathbf{B} = -\mu_0 \frac{n_e e^2}{m}\mathbf{B} \tag{A.7}$$

Version of July 4, 2022– Created July 4, 2022 - 18:59

This can be written as a second order differential equation, which is known as the London equation.

$$\nabla^2 \mathbf{B} = \frac{1}{\lambda_L^2} \mathbf{B} \tag{A.8}$$

With a simple one dimensional general solution.

$$B(x) = A \exp\left(\frac{x}{\lambda_L}\right) + B \exp\left(-\frac{x}{\lambda_L}\right) \tag{A.9}$$

where $\lambda_L = \sqrt{\frac{m}{\mu_0 n_e e^2}}$. Which for a depth $0 \leq d < \infty$ and $B_0 \equiv B(0)$, becomes the equation we wanted.

$$B(d) = B_0 \exp\left(\frac{-d}{\lambda_L}\right) \tag{A.10}$$

Appendix B

FFT's of the other data points

This appendix will show figures of FFT on the different position, from which the data points where extracted for the analysis on these different positions, including several values relevant to the plot.

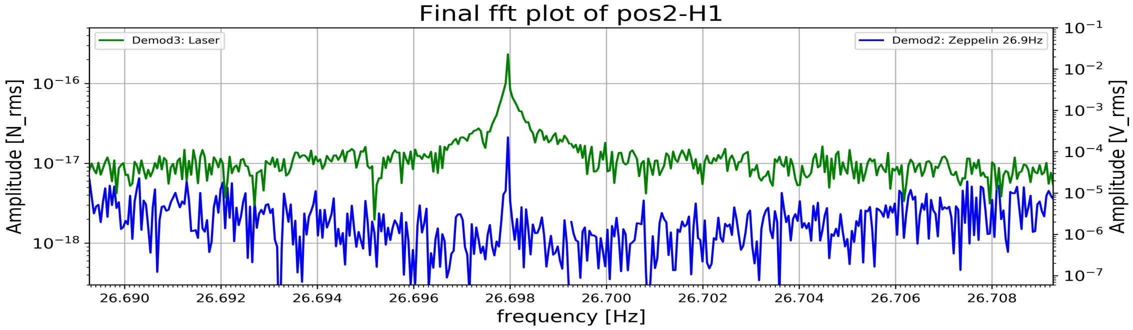

Figure B.1: *$df = 4.70 \cdot 10^{-5}$ Hz, f_{res} = 26.699269 Hz, f_{laser}=26.697955 Hz and $\Delta f_{offset} = -0.00131$*

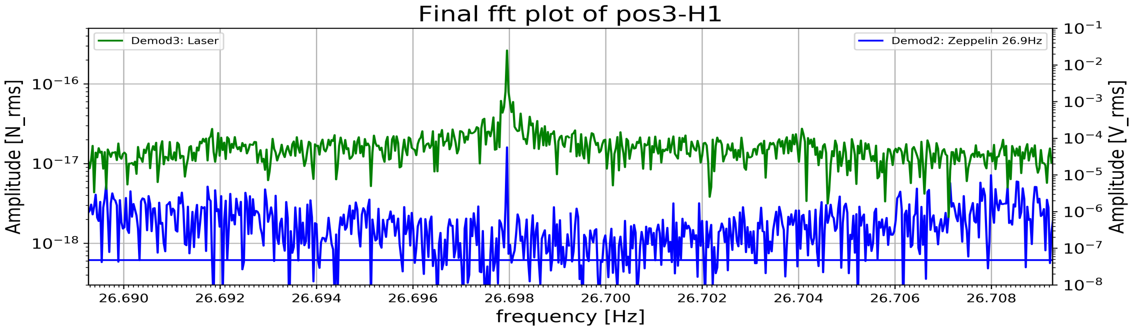

Figure B.2: $df = 3.14 \cdot 10^{-5}$ *Hz*, f_{res} = *26.699268 Hz*, f_{laser}*=26.697950 Hz and* $\Delta f_{offset} = -0.00132$ *Hz*

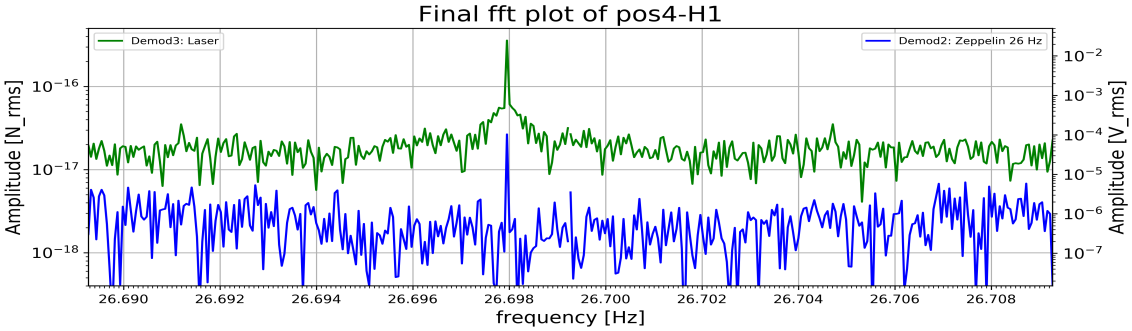

Figure B.3: $df = 5.50 \cdot 10^{-5}$ *Hz*, f_{res} = *26.699271 Hz*, f_{laser}*=26.697952 Hz and* $\Delta f_{offset} = -0.00132$ *Hz*

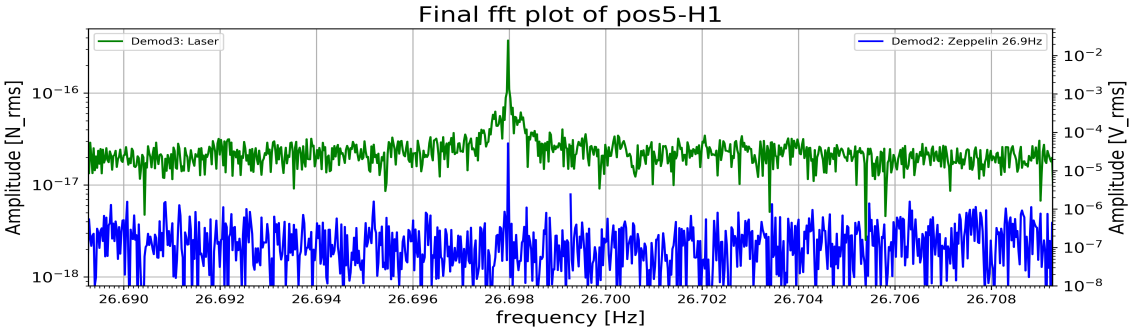

Figure B.4: $df = 2.40 \cdot 10^{-5}$ *Hz*, f_{res} = *26.699247 Hz*, f_{laser}*=26.697950 Hz and* $\Delta f_{offset} = -0.00130$ *Hz*

Version of July 4, 2022– Created July 4, 2022 - 18:59

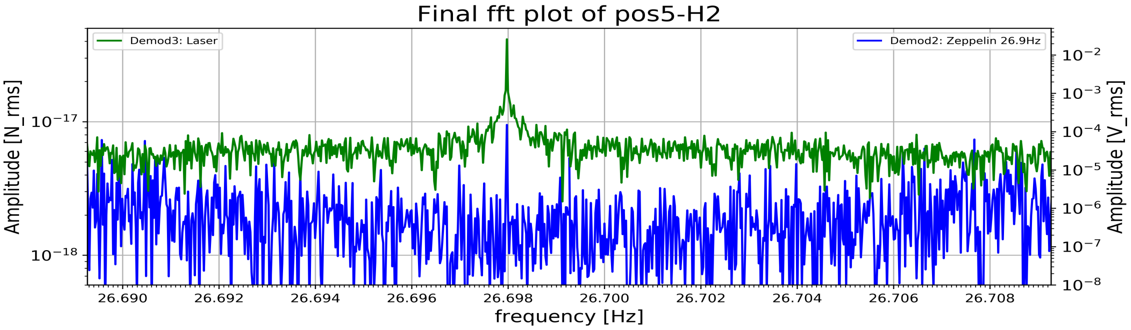

Figure B.5: *$df = 2.35 \cdot 10^{-5}$ Hz, f_{res} = 26.699246 Hz, f_{laser}=26.697951 Hz and $\Delta f_{offset} = -0.00130$ Hz*

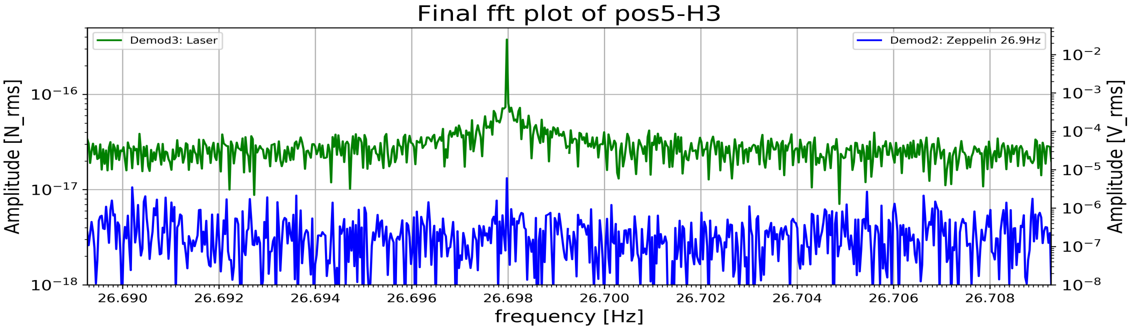

Figure B.6: *$df = 3.01 \cdot 10^{-5}$ Hz, f_{res} = 26.699247 Hz, f_{laser}=26.697951 Hz and $\Delta f_{offset} = -0.00130$ Hz*

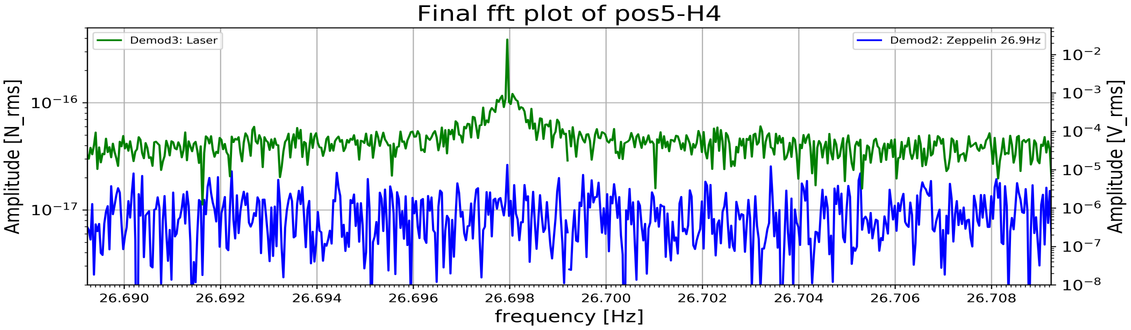

Figure B.7: *$df = 3.57 \cdot 10^{-5}$ Hz, f_{res} = 26.699236 Hz, f_{laser}=26.697949 Hz and $\Delta f_{offset} = -0.00129$ Hz*

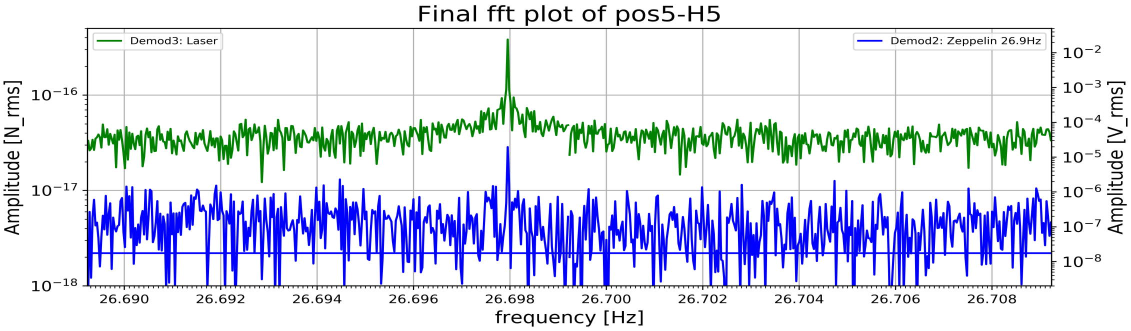

Figure B.8: $df = 3.05 \cdot 10^{-5}$ *Hz,* f_{res} *= 26.699234 Hz,* f_{laser}*=26.697952 Hz and* $\Delta f_{offset} = -0.00129$ *Hz*